Conditional blastocyst complementation of a defective Foxa2 lineage efficiently promotes generation of the whole lung

Akihiro Miura[1, 2], Hemanta Sarmah[1], Junichi Tanaka[1], Youngmin Hwang[1], Anri Sawada,[1] Yuko Shimamura[1], Yinshan Fang[1], Dai Shimizu[2], Zurab Ninish[1], Jake Le Suer[3, 4], Nicole C. Dubois[5], Jennifer Davis[6], Shinichi Toyooka[2], Jun Wu[7], Jianwen Que[1], Finn J. Hawkins[3, 4], Chyuan-Sheng Lin[8], Munemasa Mori[1] †

1 Columbia Center for Human Development and Division of Pulmonary, Allergy, Critical Care, Department of Medicine, Columbia University Medical Center, New York, NY 10032, USA.

2 Department of Thoracic, Breast and Endocrinological Surgery, Okayama University Graduate School of Medicine, Dentistry and Pharmaceutical Sciences, Okayama, 7008558, Japan.

3 The Pulmonary Center and Department of Medicine, Boston University School of Medicine, Boston, MA 02118, USA

4 Center for Regenerative Medicine, Boston University and Boston Medical Center, Boston, MA 02118, USA

5 Department of Cell, Developmental and Regenerative Biology, Icahn School of Medicine at Mount Sinai, New York, NY 10029, USA.

6 Department of Pathology, University of Washington, Seattle, WA 98109, USA.

7 Department of Molecular Biology, University of Texas Southwestern Medical Center, Dallas, TX, USA

22 8 Bernard and Shirlee Brown Glaucoma Laboratory, Department of Pathology and Cell Biology,
23 College of Physicians and Surgeons, Columbia University Irving Medical Center, New York, NY
24 10032, USA.
25
26 **† To whom correspondence should be addressed:**
27 Munemasa Mori, M.D., Ph.D.
28 650W 168th St, New York, NY 10032, USA
29 E-mail: mm4452@cumc.columbia.edu
30
31 **Abstract**
32 Millions suffer from incurable lung diseases, and the donor lung shortage hampers organ
33 transplants. Identifying the crucial lineage and the program for lung organogenesis could facilitate
34 designing whole-lung bioengineering. Using lineage-tracing mice and human iPSC-derived lung-
35 directed differentiation, we revealed that gastrulating Foxa2 lineage contributed to both lung
36 mesenchyme and epithelium formation. Interestingly, Foxa2 lineage-derived cells in the lung
37 mesenchyme progressively increased and occupied more than half of the mesenchyme niche,
38 including endothelial cells, during lung development. Foxa2 promoter-driven, conditional Fgfr2
39 gene depletion caused the lung agenesis phenotype in mice. Importantly, wild-type donor mouse
40 iPSCs injected into their blastocysts rescued this phenotype by complementing the Fgfr2-defective
41 niche in the lung epithelium and mesenchyme. Donor cell is shown to replace the entire lung
42 epithelial and robust mesenchymal niche during early chimeric lung development, resulting in
43 efficient complementation of the nearly entire lung niche at the late stage of lung development.
44 These results suggest that lung complementation based on the Foxa2 lineage is a unique model for

the progressive mobilization of donor cells into both epithelial and mesenchymal lung niches and provides crucial insights for designing new bioengineering strategies to generate whole lungs.

KEYWORDS

Lung generation

Conditional blastocyst complementation

Lung mesenchyme precursors

Mesendoderm

Lung development

Whole organ generation

57 **INTRODUCTION**

58 Tissue regeneration to treat various intractable diseases has long been challenging(Hackett
59 et al., 2010; Kemter et al., 2020; Ott et al., 2010; Petersen et al., 2010; Wang, 2019). Organ
60 bioengineering strategy based on recellularizing tissue-specific progenitors into the decellularized
61 scaffolds, induced pluripotent stem cell (iPSC)-derived organoids, or 3d-bioprinters are the next-
62 generation tissue transplant therapies(Guyette et al., 2014; Kotton and Morrisey, 2014; Petersen et
63 al., 2010; Tian et al., 2021). Even with these techniques, however, the mammalian lung is one of
64 the most difficult organs to replicate because of its anatomical complexity and cellular diversity.
65 It contains hundreds of airway branches and a thin micron-sized alveolar layer of inflated and well-
66 vascularized alveoli composed of billions of cells from more than 50 different cell types(Crapo et
67 al., 1982; Kotton and Morrisey, 2014; Stone et al., 1992; Travaglini et al., 2020). Donor organs for
68 lung transplantation are in short supply worldwide, but the technology does not exist to generate
69 whole lungs composed of tissue-specific epithelial and mesenchymal cells, including endothelial
70 cells. Lungs grow fully only through natural lung development.

71

72 During development, lung epithelial and mesenchymal precursors interact to initiate an
73 elaborate developmental program of organogenesis that includes specification, pattern formation,
74 progenitor cell expansion, and differentiation. The lung epithelial cells are derived from the foregut,
75 definitive endoderm (DE) derivatives, classically labeled by Sox17 and Forkhead Box A2
76 (Foxa2)(Green et al., 2011; Huang et al., 2014). Multiple genetic studies using Sonic Hedgehog
77 (Shh) Cre lineage-tracing mice have also shown that the entire Nkx2-1+ lung and tracheal
78 epithelial primordium arises from Shh^+ DE.

79 The lung mesenchyme primordium is derived from Wnt2^{+} Isl1^{+} cardiopulmonary
80 progenitors (CPP). CPP is the derivative of Osr1^{+} Nkx6-1^{+}Barx1^{-} Wnt4^{low} foregut lung mesoderm
81 that arises from lateral plate mesoderm (LPM)(Han et al., 2020). While DE and LPM arise from
82 primitive streaks (PS) during gastrulation, the exact lineage origin of LPM has been a complete
83 mystery.
84 Mesendoderm is a bipotent transitional state between the PS and nascent mesoderm labeled
85 by Mixl1, Pdgfrα, and Brachyury (T) during gastrulation that can give rise to both DE and
86 mesoderm(Hart et al., 2002; Tada et al., 2005). Although it was speculated that mesendoderm
87 might form LPM and DE, there have been no conclusive genetic studies on whether mesendoderm
88 gives rise to both lung epithelium and mesenchyme. Pdgfrα is expressed in the epiblast-derived
89 mesendoderm, the primitive endoderm (PrE), and its extra-embryonic endoderm derivatives, such
90 as parietal and visceral endoderm, around E5.5~E7.5. Foxa2 plays a pivotal role in alveolarization
91 and airway goblet cell expansion(Wan et al., 2004), while there was a significant knowledge gap
92 regarding Foxa2 lineage during lung development.
93
94 Blastocyst complementation (BC) has been proposed as a promising option for tissue-
95 specific niche complementation(Chen et al., 1993). This unique technology has been further
96 developed into intra- and interspecies organ generations such as kidney, pancreas, and blood
97 vessels(Hamanaka et al., 2018; Kobayashi et al., 2010; Usui et al., 2012; Yamaguchi et al., 2017).
98 However, the production of entire organs, including tissue-specific epithelium and mesenchyme,
99 including endothelium, was still difficult because endothelium significantly impacts the other
100 organs. Unfortunately, even with BC, the lungs produced were non-functional and very inefficient,
101 and in addition, the chimeric lungs contained a substantial amount of host-derived tissue(Kitahara

102 et al., 2020; Li et al., 2021; Wen et al., 2021). Previously, we established the conditional blastocyst
103 complementation (CBC) approach, which targets specific lineages complemented by donor
104 pluripotent stem cells(Mori et al., 2019). Using lineage-specific drivers of lung endoderm in CBCs
105 avoids the effects of genetic manipulation in non-target organs for the generation of empty organ
106 niches that lead to functional chimeric lung generation(Mori et al., 2019). However, most of the
107 lung mesenchyme and endothelium were still derived mainly from the host cells, which was the
108 severe limitation of CBC(Mori et al., 2019). Given that the CBC approach targeted endodermal
109 lungs, we speculated that this limitation was due to a significant gap in our knowledge of the origin
110 of all lung cell types, especially pulmonary mesenchyme, including endothelium. In particular, the
111 complementation of endothelium is a critical issue for overcoming hyperacute rejection after lung
112 transplantation. To overcome this critical issue, we explored the origin and the program of whole
113 lung epithelium and mesenchyme, the major components of the lung.

114 We hypothesized that targeting a single bona fide lung generative lineage (BFL) may
115 facilitate the designing of the entire lung generation. BFL is based on the strategy for vacating the
116 desired niche by lineage-specific gene depletion to be complemented by donor cells after injecting
117 them into the host blastocysts. The lineage is not necessarily lung-specific but rather based on
118 emptying or mitotically defective in the desired lineage by gene depletion.

119 We found that the Foxa2 lineage functions as a BFL in CBC. Although the Foxa2 lineage
120 did not label the entire lung cells during lung development, the mitotically-defective Foxa2 lineage
121 promoted efficient whole-lung complementation by donor cells.

122

123 **RESULTS**

124 **Pdgfrα^{+} lineage during gastrulation gives rise to the entire lung mesenchyme.**

125 To determine the origin of LPM and pulmonary endothelium for the whole lung generation
126 via BFL, we performed lung mesenchyme precursor lineage-tracing analysis using *Pdgfrα*$^{CreERT2/+}$;
127 *Rosa*$^{tdTomato/+}$ mice. Surprisingly, tamoxifen injection at E5.5 labeled the entire lung mesenchyme
128 with tdTomato at E14.5 (Figures 1A and 1B). This result suggested that the origin of the whole
129 lung mesenchyme is the Pdgfrα lineage around early-to-mid-streak-stage embryos. tdTomato
130 labeled the entire pulmonary mesenchyme, including Sma$^+$ airway smooth muscle cells, Pdgfrβ$^+$
131 pulmonary mesenchyme, and VE-cadherin$^+$ vascular endothelial cells (Figure 1B). In addition, the
132 Pdgfrα lineage only partially labels the lung epithelium (Figure 1B, arrows), suggesting that the
133 contribution of the Pdgfrα lineage to the lung endoderm is low. It suggests that Pdgfrα is difficult
134 to define as a BFL because of its low contribution to the lung epithelium.
135

136 **Foxa2 lineage labels Pdgfrα$^+$ mesendoderm niche during mouse development**

137 Single-cell RNA-seq (scRNA-seq) analysis using Foxa2-Venus fusion protein reporter
138 mice indicated that the Foxa2 lineage might give rise to LPM and DE (Scheibner et al., 2021).
139 Given that Foxa2 and Pdgfrα are expressed during the conversion from mesendoderm to
140 mesenchyme(Artus et al., 2010; Kopper and Benvenisty, 2012; Scheibner et al., 2021; Tada et al.,
141 2005), we used Foxa2-lineage tracing mice (*Foxa2*$^{Cre/+}$; *Rosa*$^{tdTomato/+}$)(Horn et al., 2012) to
142 determine whether the Foxa2-lineage would label Mixl1$^+$ or Pdgfrα$^+$ mesendoderm around
143 E6.25~7.0 during gastrulation. Notably, Foxa2-lineage-driven tdTomato labels a part of the
144 Pdgfrα$^+$ mesendoderm of the primitive streak (PS) around E6.25~E6.5 relatively early-streak-stage
145 embryos (Figure 1C, arrow). In the E6.5~E7.0 mid-to-late-streak-stage PS region (Figure 1D,
146 dotted lines), Foxa2-lineage-derived tdTomato were found in the PS and Pdgfrα$^+$ adjacent nascent
147 mesoderm, suggesting that Foxa2 lineage-labeled Pdgfrα$^+$ cells ingresses from PS to nascent

148 mesoderm regions (Figure 1D, arrowheads). These data are reminiscent of the definition of
149 mesendoderm (Hart et al., 2002; Tada et al., 2005). Our result indicates that the Foxa2 lineage-
150 labeled Pdgfrα$^+$ cells are the mesendoderm, most likely the derivative of posterior epiblasts, since
151 Foxa2 is expressed only in the posterior epiblasts before gastrulation (Scheibner et al., 2021).
152 Further immunostaining analysis of the sequential sections of mid-streak-stage E6.5~6.75 embryos
153 confirmed that the Foxa2 lineage appeared in the distal portion of Mixl1-weakly-positive
154 mesendoderm (Figures 1E and 1F, arrows) at anterior primitive streak (APS) besides the Foxa2
155 protein-expressing DE (Figures 1E and 1F, arrowheads). Based on our Pdgfrα$^+$ lineage tracing
156 data, we further examined whether Foxa2-lineage would label lung mesenchyme.
157

158 **Foxa2-lineage labeling increased during lung development, leading to occupy the entire lung**
159 **epithelium and half of the lung mesenchyme, including lung endothelium**

160 Foxa2-lineage tracing mice (*Foxa2*$^{Cre/+}$; *Rosa*$^{tdTomato/+}$) faithfully target Nkx2-5$^+$ cardiac
161 progenitors associated with the origin of Wnt2$^+$ Isl1$^+$ CPP(Bardot et al., 2017; Peng et al., 2013)
162 lung mesenchyme. However, there was no conclusive evidence of whether Foxa2-lineage can give
163 rise to Wnt2$^+$ Isl1$^+$ CPP(Bardot et al., 2017; Peng et al., 2013). Using the Foxa2-lineage tracing
164 mice, we found from immunostaining that Foxa2 lineage labeling occupies the entire lung
165 epithelium and most of the lung mesenchyme at E16.5 (Figures 2A-C). Quantitative analyses by
166 flow cytometry in the E14.5 developing lungs of Foxa2-lineage tracing mice showed that Foxa2-
167 lineage labeled almost the entire lung epithelium (93.3%± 2.00) and the partial lung mesenchyme
168 (24.2%± 5.51), including endothelial cells (16.8 %± 5.12) (Figure 2D). Contrary to expectations,
169 Foxa2-lineage labeled cells increased dramatically throughout lung development (Figure 2E). In
170 adulthood, the Foxa2-lineage labeling reached about 99.97%± 0.0578 in lung epithelium, 51.27%±

171 1.72 in lung mesenchyme, and 59.97%± 8.44 in lung vascular endothelial cells, with more than
172 two-fold change in the lung endothelium, compared with E14.5 (Figure 2E). Morphometric
173 analysis of immunostaining further confirmed that Foxa2 lineage marked about 30% of E14.5
174 multiple cell types of lung mesenchyme: Sma$^+$ smooth muscle cells (24.9%± 8.50), VE-cadherin$^+$
175 (39.3%± 12.5) or Pecam1$^+$ (36.6%± 11.1) endothelial cells, and Pdgfrβ$^+$ pericytes of the pulmonary
176 arteries and pulmonary veins (41.4%± 10.5) (Figures 1F and 1G). Interestingly, no clear Foxa2
177 protein level expression was observed in the mesenchyme of the embryonic lungs (Figure S1A),
178 consistent with previously reported Foxa2 protein expression patterns(Wan et al., 2004). However,
179 the LungMAP deposited single-cell RNA-seq database analysis showed a sporadic Foxa2
180 transcriptional expression pattern in developing lung mesenchyme, particularly in proliferating
181 endothelium, on E15.5 and E17.5 (Figure S1B). We confirmed *Foxa2* transcriptional expression
182 in lung mesenchyme by in situ hybridization analysis on E18.5 (Figure S1C and S1D). The
183 expression was detected mostly in tdTomato positive but low frequency in the negative cells,
184 which indicates that lung mesenchyme spontaneously expressed *Foxa2* at a transcriptional level
185 and turn on tdTomato during lung development. We also sorted the cell fraction of CD45$^-$ CD31$^-$
186 EPCAM$^-$ tdTomato$^+$ and CD45$^-$ CD31$^-$ EPCAM$^-$ tdTomato$^-$ from developing lung mesenchyme at
187 E18.5. We observed a slight increase in the relative expression of *Foxa2* in the tdTomato$^+$ fraction
188 of embryonic lung mesenchyme, which most likely contributed to the labeling in the Foxa2-lineage
189 tracing mice (Figure S1E). These results suggest pulmonary mesenchymal progenitor cells turned
190 on Foxa2 expression slightly at the mRNA level rather than the protein level, which led to a gradual
191 increase in Foxa2 lineage labeling. Furthermore, tdTomato$^+$ endothelial cells were found to have
192 a slightly higher proliferative capacity than tdTomato$^-$ cells (Figure S1F). These results suggest
193 that Foxa2 lineage$^+$ pulmonary mesenchymal appeared during lung development, and lineage

194 labeling gradually increased compared to Foxa2$^-$ lung mesenchyme progenitors throughout lung
195 development.
196
197 **Co-development of endodermal and mesodermal lung progenitors derived from MXIL1$^+$**
198 **PDGFR α^+ FOXA2$^+$ mesendoderm in the directed differentiation protocol using hiPSC**
199 To determine whether Foxa2 or Pdgfrα mesoderm is an evolutionarily well-conserved
200 niche that can give rise to both pulmonary endoderm and mesoderm, we modified a previously
201 reported protocol to establish a pulmonary endoderm-mesoderm co-developmentally directed
202 differentiation protocol(Chen et al., 2017; Gotoh et al., 2014; Hawkins et al., 2017; Huang et al.,
203 2014; Konishi et al., 2016) (Figure 3A). With this optimized protocol, various hiPSC lines were
204 found to efficiently induce a lung bud-like appearance, indicated by NKX2-1+, in lung epithelial
205 cells(Gotoh et al., 2014; Konishi et al., 2016). We found that on day 10, TBX4$^+$ lung mesenchyme
206 emerged and surrounded the NKX2-1$^+$SOX9$^+$ lung epithelium (Figure 3B and 3C). The qPCR
207 kinetics analyses across the time point further supported the appearance of lung mesenchyme,
208 represented by LPM marker expression peaked on day6~8; *OSR1, FGF10, BMP4, PDGFRα*, and
209 smooth muscle cell markers peaked on day8~10; *ACTA2* and *PDGFRβ*, and CPP markers peaked
210 on day8~12; *ISL1, WNT2, FOXF1,* and *TBX4*, peaked on days 10~14 simultaneously with
211 pulmonary epithelial markers, *NKX2-1* and *CPM* (Figure 3D).
212 In this differentiation protocol, NKX2-1$^+$ lung endoderm and WNT2+TBX4$^+$ lung
213 mesoderm were derived from the anteroventral endoderm and mesoderm at day 15 after Activin-
214 mediated definitive endoderm and LPM induction, respectively(Chen et al., 2017; Huang et al.,
215 2014). During primordial streak induction from day0 to day3, cell surface markers of PDGFRα
216 and EPCAM and intracellular FOXA2 and MIXL1 kinetics were analyzed by flow cytometry

217 every 12 hours (Figure 3E). Briefly, 12 hours after the Activin induction, more than 60% of the
218 EPCAM^{+}PDGFRα^{-} primitive streak first turned on MIXL1, the mesendoderm marker(Hart et al.,
219 2002; Tada et al., 2005). Subsequently, the epithelial-mesenchymal transition occurred 24 hours
220 later, as represented by the PDGFRα induction in EPCAM^{+}MIXL1^{+} mesendoderm. After 36 hours,
221 more than 90% of MIXL1+EPCAM+ mesoderm cells expressed PDGFRα. At the same time,
222 expression of FOXA2 appeared in some of those mesoderm cells (Figures 3E and 3F). Thereafter,
223 PDGFRα expression decreased, and 72 hours later, mutual FOXA2 induction appeared when
224 EPCAM^{+}FOXA2^{+} DE and EPCAM^{-}FOXA2^{-} LPM were presented (Figure 3G). The dynamics of
225 MIXL1, PDGFRα, and FOXA2 were further revealed by qPCR analysis (Figure 3H). These results
226 suggest that PDGFRα^{+} and FOXA2^{+} lineage are redundant but distinct stages of mesoderm
227 development. It can give rise to both endoderm and mesoderm lung cells conserved in mouse
228 development and human-directed differentiation (Figure S4A).
229

230 **Foxa2-driven Fgfr2 conditional knockout showed a lung agenesis phenotype**

231 The evolutionary-conserved Foxa2-lineage^{+} mesendoderm forms endodermal and
232 mesodermal lung niches, suggesting that it may function as a BFL to generate the entire lungs after
233 donor cells are injected into the vacant niche in the Foxa2 lineage. To explore this possibility, CBC
234 was performed using Foxa2-driven Fgfr2-conditional knockout mice (*Foxa2*$^{Cre/+}$; *Fgfr2*$^{flox/flox}$,
235 hereafter, *Foxa2*$^{Cre/+}$; *Fgfr2*^{cnull}). Mitotic signaling via Fgfr2 is required for both lung epithelium
236 and mesenchyme, and systemic knockout mice of Fgf10 or Fgfr2 exhibit a phenotype of lung
237 agenesis(Arman et al., 1999; De Langhe et al., 2006; De Moerlooze et al., 2000; Sekine et al.,
238 1999). Based on the results of Foxa2 lineage tracking and the need for Fgfr2 signaling, it was
239 predicted that *Foxa2*$^{Cre/+}$; *Fgfr2*^{cnull} mice would be used to generate vacant niches in both lung

240 epithelium and mesenchyme. Indeed, they exhibited a lung agenesis phenotype (Figures S2A-S2C).
241 However, we did not observe agenesis phenotype in other major internal organs related to the
242 Fgfr2 systemic knockout phenotype (Figure S2D) (Arman et al., 1999; De Langhe et al., 2006; De
243 Moerlooze et al., 2000; Sekine et al., 1999).
244

245 **Generation of the entire lungs in *Foxa2*-driven *Fgfr2*-deficient mice via CBC**

246 To examine whether donor cells complement the lung agenesis phenotype, we generated
247 nGFP^{+}iPSCs from Rosa$^{nT\text{-}nG}$ mice (hereafter, nGFP^{+}iPSCs) via Sendai virus-mediated
248 reprogramming(Huang et al., 2014). nGFP^{+}iPSCs were injected into mouse blastocysts (Figure
249 4A), and chimerism was analyzed at E17.5. Strikingly, donor nGFP^{+}iPSCs generated whole lungs
250 in *Foxa2*$^{Cre/+}$; *Fgfr2*^{cnull} mice, but general chimerism in other organs were diverse (Figure 4B, S3A,
251 and Table 1). Importantly, almost the entire lung epithelial, mesenchymal, and endothelial cell
252 population at E17.5 was composed exclusively of nGFP^{+}iPSCs (Figures 4C and S3B). In contrast,
253 wild-type, Shh-driven heterozygous, or knockout mice showed about 50-70% chimerism in the
254 mesenchymal and endothelial lineages of the lung (Figures 4C and 4D). Interestingly, although
255 tdTomato^{+} Fgfr2 knockout mesenchymal cells remained in early lung development at E14.5
256 (Figure S3C and Table 2), the percentage of Ki67^{+} proliferating cells was significantly higher in
257 GFP^{+} donor cells compared to tdTomato^{+} host cells (Figures 4E – 4G). These results suggest that
258 generating an Fgfr2 deficient niche in the host Foxa2 lineage-derived lung mesenchyme is efficient
259 for donor iPSCs recruitment in the defective Foxa2 lineage mesenchyme niches.
260

261 **DISCUSSION**

262 The presence of committed organ precursors capable of contributing to multi-embryonic
263 layers after pluripotent epiblast formation has been assumed, but the identity and origin of the lung
264 precursors needed to be better defined. Although the Foxa2 lineage could not give rise to the entire
265 lung cells that served as a BFL, we have identified a Foxa2 lineage that provides a significant
266 stepping stone for facilitating whole lung generation during mouse development. Since donor cells
267 formed about 50~80% chimerism in the complemented lung mesenchyme niches at E14.5 (Table
268 1) and endogenous Foxa2 lineage forms only 20%~30% in the lung mesenchyme at E14.5, Fgfr2
269 defects at the Foxa2 lineage in early lung development are important but not sufficient for the
270 complete lung mesenchyme niche complementation. We showed that losing Fgfr2 expression in
271 Foxa2 lineage cells resulted in lower proliferative ability than donor cells during the lung
272 complementation (Figure 4F).

273 Lung epithelial cell precursors were well-known to be Shh$^+$ DE in the lung development
274 field(Cardoso and Kotton, 2008; Christodoulou et al., 2011; Harris et al., 2006; Kadzik and
275 Morrisey, 2012; Tian et al., 2011; Weaver et al., 1999; Xing et al., 2008), and indeed, the Shh-
276 lineage traces putative DE-derived epithelial lineage but little lung mesenchyme (Figure S3D).
277 Targeting the endodermal lung lineage driven by Shh was sufficient for lung epithelial
278 complementation but insufficient to generate whole lungs, and host-derived cells remained
279 substantially in the mesodermal lung component (Mori et al., 2019).

280 In contrast to lung epithelium precursors, the orderly commitment and the origin of the
281 entire pulmonary mesenchyme were not defined well. We showed that gastrulating Pdgfrα-lineage
282 is the origin of the entire lung mesoderm, including endothelium (Figures 1A and 1B)(Mori et al.,
283 2019). Furthermore, Foxa2 or Pdgfrα lineage labels a population primarily comprised of the
284 earliest specified precursors in the Mixl1$^+$ mesendoderm niche, which can be identified in vivo and

285 in human iPSC cell-derived directed differentiation protocol. Our findings, summarized in Figure
286 S4, pinpoint the lineage hierarchy of specified lung precursors in gastrulating mesendoderm,
287 further supported by the scRNA-seq analysis in early embryonic development(Pijuan-Sala et al.,
288 2019) (Figure S4B).

289 As previously indicated that nascent mesoderm differentiation into a CPP fate(Bardot et
290 al., 2017; Devine et al., 2014; Ng et al., 2022; Peng et al., 2013), we clarified the orderly
291 mesendoderm progression of gene expression, Mixl1, Pdgfrα, and Foxa2, and lung progenitor-
292 related markers that parallels the commitment of Foxa2^{+} Pdgfrα^{+} mesendoderm to an LPM and
293 DE fate in the lung directed differentiation protocol using human iPSC (Figure S4). Our lineage
294 tracing analysis also highlighted the unanticipated Foxa2 lineage program, the progressive increase
295 of lineage labeling by spontaneous expression of *Foxa2 mRNA* that occupies more than half of the
296 lung mesenchyme during lung development. Foxa2-lineage^{+} lung mesenchyme is a part of Pdgfrα
297 lineage^{+} cells, potentially providing a unique competitive developmental niche during lung
298 development. Further analyses using Foxa2CreERT2 lineage tracing mice are required to clarify
299 it. Intriguingly, the Foxa2 lineage^{+} mesenchyme did not show any discrete fates that would predict
300 anatomical localization—depleting Fgfr2 in the Foxa2 lineage results in the loss of the Fgfr2
301 mitogen-mediated function of Foxa2 lineage^{+} lung mesenchyme, which leads to the loss of
302 proliferative ability in most host lung mesenchyme. The Foxa2 lineage labeling in lung
303 mesenchyme is around 20% at E14.5 (Figure. 2D and 2E). Moreover, the donor cell
304 complementation in lung mesenchyme at E14.5 still holds host-derived lung mesenchyme but
305 decreases at E17.5. These results indicate that the defective Foxa2 lineage is critically important
306 for efficient lung complementation.

307 An unambiguous proof of the developmental origins of patterned organs is critical for
308 developing regenerative strategies and a better understanding of the genes responsible for
309 congenital malformations. For the future development of whole lung generation via CBC using
310 human iPSCs, the human-derived developmental program modification to match the host animals
311 is the key. More broadly, our studies offer a new paradigm that can apply to modeling various
312 congenital lung diseases and future autologous transplantation therapies using iPSC in the near
313 future.
314

315 **Acknowledgments**

316 We thank Zurab Ninish for his technical assistance. We sincerely appreciate the generous support
317 from Dr. Hiromitsu Nakauchi at Stanford University and the considerate support and scientific
318 input from Dr. Wellington Cardoso at the Columbia Center for Human Development (CCHD) and
319 the members of Cardoso's lab and CCHD. We acknowledge the support from the CCHD Medicine
320 Microscopy core (MMC), Columbia Stem Cell Initiative (CSCI) Flow Cytometry core (SONY
321 MA900), and Genetically Modified Mouse Model Shared Resource (GMMMSR) for blastocyst
322 injection. This work was funded by NIH-NHLBI 1R01 HL148223-01, DoD PR190557, PR191133
323 to M. M., JSPS202080340, and The Uehara Memorial Foundation to A. M.
324

325 **Author contributions**

326 A.M. and M.M. designed all experiments; Z.N. and A.M. maintained mutant mice for the injection;
327 C.S.L. performed blastocyst injection and embryo transfer; J.T., A.S., Y.S., Y.H., H.S., supported
328 lineage-tracing, chimera analyses, and genotyping; H.S., D.S., and S. T. helped to generate mouse
329 and human iPSCs, J.S. and F.H. kept human iPSC-directed differentiation, N.D. provided

330 Foxa2$^{Cre/+}$ mice, A.M. and M.M. wrote the paper; Y.H., H.S., J.W., J.Q., and F.H. gave crucial

331 insights on the experiments and the manuscripts. There is no competing financial interest.

332

333 **Declaration of interests**

334 The authors declare no competing interests.

335

336

337 **FIGURES**

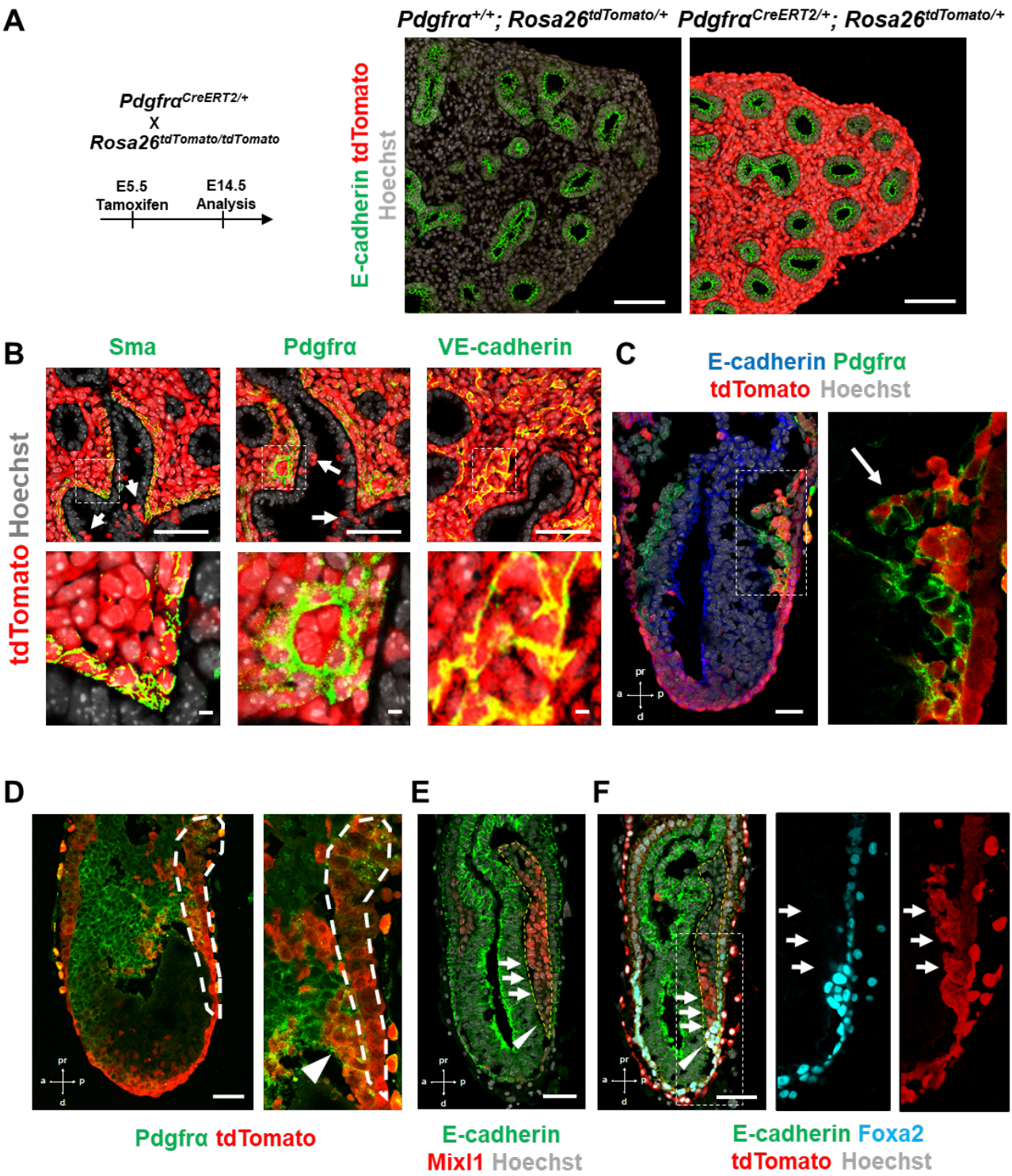

338

339

340 **Figure 1. Pdgfrα lineage during gastrulation is the origin of the entire pulmonary**
341 **mesenchyme.** (A) Left: Schematic of Tamoxifen administration (A-B). Representative
342 Immunofluorescence (IF)-confocal imaging of E14.5 *Pdgfrα*$^{CreERT2/+}$*; Rosa26*$^{tdTomato/+}$ lineage
343 tracing mouse lungs (A, B). Tamoxifen administration at E5.5 labels Pdgfrα-lineage-driven
344 tdTomato (red) in the entire lung mesenchyme (A), including Sma^{+} airway smooth muscle cells,
345 Pdgfrα^{+} mesenchyme, and VE-cadherin^{+} capillaries (B). Pdgfrα-lineage also labeled a low
346 proportion of epithelial cells (B, white arrows). Enlarged box: dotted box. Cre^{-} littermate control
347 (A, middle panel) (*n = 3* per group). Scale bars: A, B = 100, 500μm. (C-F) Representative IF-
348 confocal imaging of E6.25 (C), E7.0 (D), and E6.5 (E, F) from *Foxa2*$^{Cre/+}$*; Rosa26*$^{tdTomato/+}$ mice. E-
349 cadherin indicates epiblasts (C-F): (C) Foxa2-lineage (red) labeled Pdgfrα (green) expressing
350 mesendoderm (arrow). (D) Foxa2-lineage labeled Pdgfrα^{+} cells and ingresses from primitive
351 streak (PS) (dotted lines) to nascent mesoderm regions (arrowhead). (E) Mixl1 (red) expression in
352 PS (yellow dotted area). (F) Sequential section of E: Enlarged box: Foxa2-lineage (red) marked
353 the distal portion of the arteriolarizing PS that is a part of the MIxl1^{dim+} mesendoderm (E-F,
354 arrowheads). (*n = 3* per group). Scale bars = 50μm.

355

356

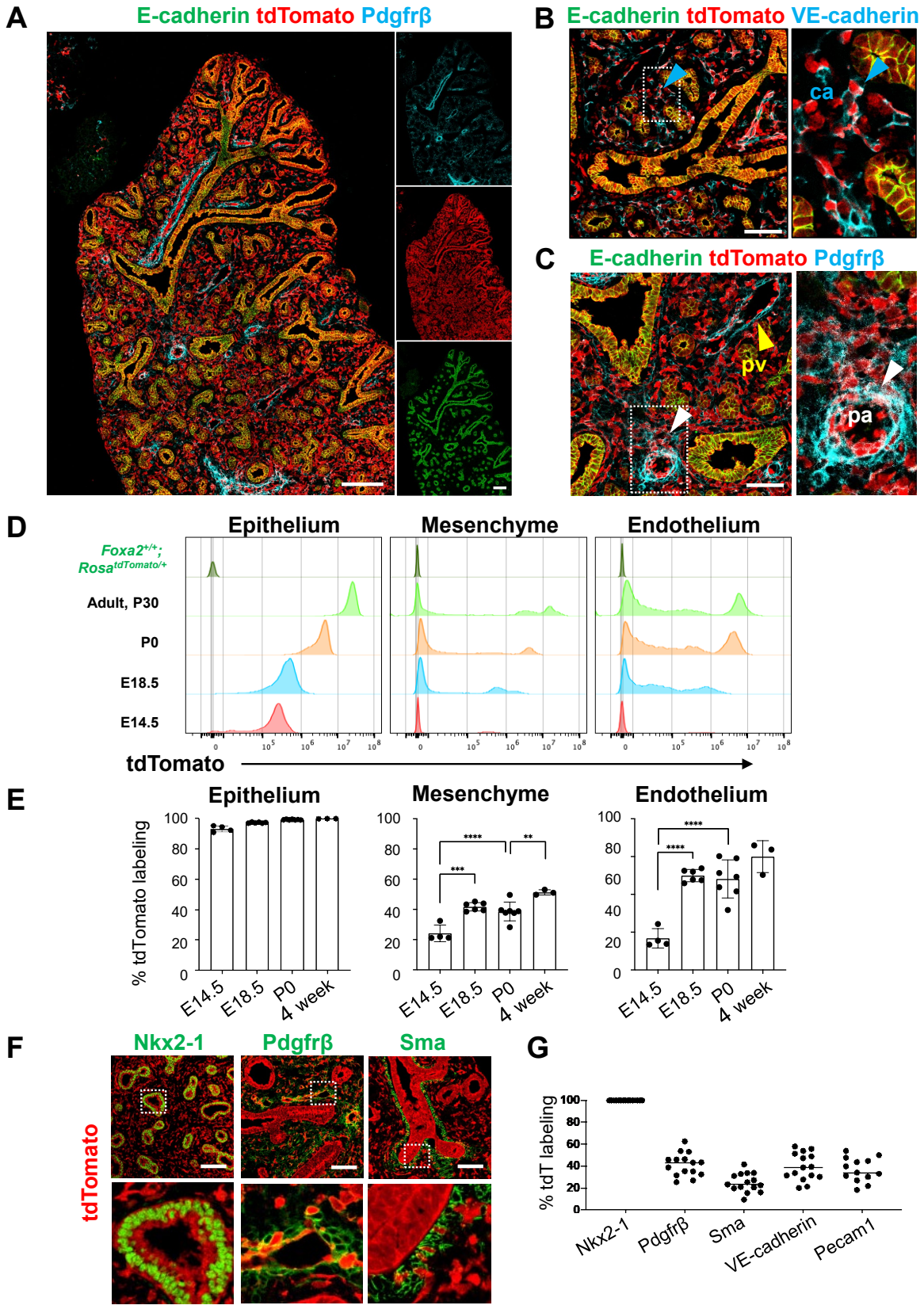
A
E-cadherin tdTomato Pdgfrβ
B
E-cadherin tdTomato VE-cadherin
ca
C
E-cadherin tdTomato Pdgfrβ
pv
pa
D
Epithelium
Mesenchyme
Endothelium
Foxa2+/+; Rosa tdTomato/+
Adult, P30
P0
E18.5
E14.5
tdTomato
E
Epithelium
Mesenchyme
Endothelium
% tdTomato labeling
E14.5
E18.5
P0
4 week
F
Nkx2-1
Pdgfrβ
Sma
tdTomato
G
% tdT labeling
Nkx2-1
Pdgfrβ
Sma
VE-cadherin
Pecam1

357

358 **Figure 2. Foxa2-lineage gradually increased during lung development and labeled the entire**
359 **lung epithelium and half of the mesenchyme.** (A-C) IF-confocal imaging of E16.5 *Foxa2*$^{Cre/+}$*;*
360 *Rosa*$^{tdTomato/+}$ embryonic lung: (A) Foxa2-lineage (red) labeled E-cadherin^{+} lung epithelium (green)
361 entirely and Pfgfrβ^{+} mesenchyme (cyan) partially. (B) Foxa2-lineage partially labeled VE-
362 cadherin^{+} capillary (ca) (enlarged box, blue arrowhead). (C) Foxa2-lineage labeled Pdgfrβ^{+} smooth
363 muscle cells of the pulmonary artery (pa) (enlarged box, white arrowhead) and pulmonary vein
364 (pv, yellow arrowhead). Scale bars (A), (B), and (C) = 200μm, 100μm, and 100μm, respectively.
365 (D and E) Representative histograms and the graphs of FCM quantitative analyses for CD31^{-}
366 Epcam^{+} lung epithelium, CD31^{-}Epcam^{-} mesenchyme, and CD31^{+}Epcam^{-} endothelium at E14.5,
367 E18.5, P0, and four weeks adult (n = 4, 6, 7 and 3, independent biological replicates, respectively)
368 of *Foxa2*$^{Cre/+}$*; Rosa*$^{tdTomato/+}$ mouse lungs. The gradual increase of % tdTomato^{+} lineage labeling
369 in both lung mesenchyme and endothelium. Statistical analysis: one-way ANOVA with the Tukey
370 post hoc test.; statistically significant if $^{*}P < 0.05$, $^{**}P < 0.01$, $^{***}P < 0.001$, $^{****}P < 0.0001$. (F-
371 G) IF-confocal imaging of E14.5 *Foxa2*$^{Cre/+}$*; Rosa*$^{tdTomato/+}$ embryonic lungs. tdTomato labeled entirely
372 with lung epithelial markers Nkx2-1(left) but a relatively low proportion of mesenchyme (Pdgfrβ:
373 middle, and Sma: right). (n = 3 per group). Scale bars = 50μm. Graphs in (G): The morphometric
374 analysis: % of Foxa2-lineage labeling in Nkx2-1^{+}epithelial, Pdgfrβ^{+}mesenchyme, Sma^{+}airway
375 smooth muscle, VE-Cadherin^{+} capillaries, or PECAM1^{+} arteries from E14.5 *Foxa2*$^{Cre/+}$*; Rosa*$^{tdTomato/+}$
376 lungs. (n = 3 per biological replicates, 5 fields per group).
377
378

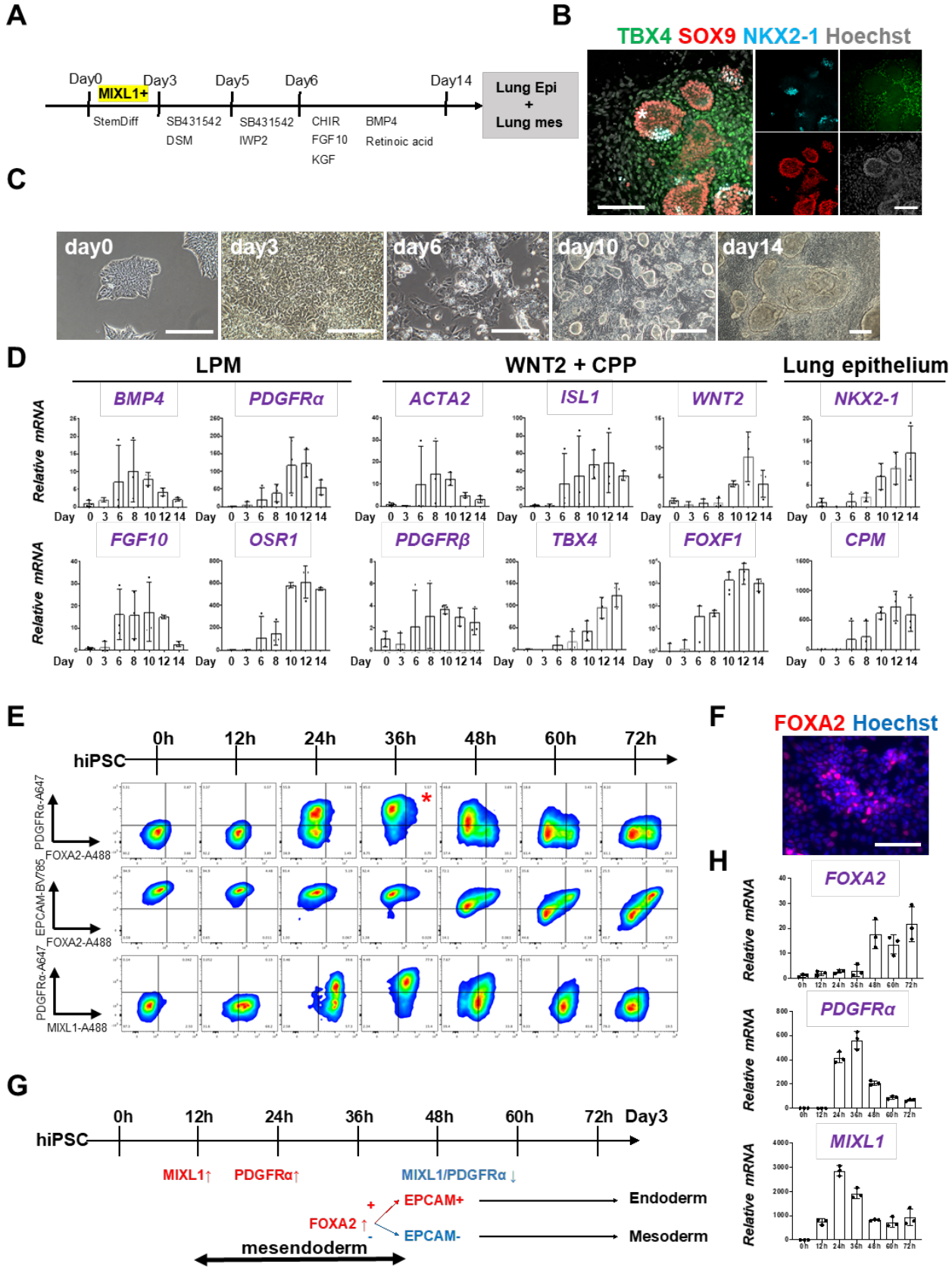
A
Day0
MIXL1+
Day3
Day5
Day6
Day14
StemDiff
SB431542
DSM
SB431542
IWP2
CHIR
FGF10
KGF
BMP4
Retinoic acid
Lung Epi
+
Lung mes
B
TBX4 SOX9 NKX2-1 Hoechst
C
day0
day3
day6
day10
day14
D
LPM
WNT2 + CPP
Lung epithelium
BMP4
PDGFRα
ACTA2
ISL1
WNT2
NKX2-1
FGF10
OSR1
PDGFRβ
TBX4
FOXF1
CPM
Relative mRNA
Day 0 3 6 8 10 12 14
E
hiPSC
0h
12h
24h
36h
48h
60h
72h
PDGFRα-A647
FOXA2-A488
EPCAM-BV785
MIXL1-A488
F
FOXA2 Hoechst
H
FOXA2
PDGFRα
MIXL1
Relative mRNA
G
hiPSC
0h
12h
24h
36h
48h
60h
72h
Day3
MIXL1↑
PDGFRα↑
MIXL1/PDGFRα↓
FOXA2↑
EPCAM+
EPCAM-
Endoderm
Mesoderm
mesendoderm

379

380 **Figure 3. Co-development of endodermal and mesodermal lung progenitors derived from**
381 **MXIL1$^+$ PDGFR α^+ FOXA2$^+$ mesendoderm in the directed differentiation protocol using**
382 **hiPSC.** (A) Schematic culture protocol of hiPSC-derived endodermal and mesodermal lung
383 progenitor cell co-differentiation. (B) Representative IF-confocal imaging of differentiating
384 hiPSCs at day 10 culture. Lung epithelium (NKX2-1), distal lung bud epithelium (SOX9),
385 mesenchyme (TBX4), and nucleus (Hoechst) markers. The budding structures expressed SOX9
386 and partially NKX2-1 (asterisk), and monolayer cells expressed TBX4. (C) Representative phase-
387 contrast images of the directed differentiation time course (D) qRT-PCR analyses of lung
388 mesenchyme and epithelium markers in time course according to the protocol shown in (A). Each
389 plot showed a different biological experiment (n = 3 independent experiments). (E) FCM-based
390 protein kinetic analyses during DE and LPM induction; MIXL1 expression preceded compared to
391 PDGFRα or FOXA2. FOXA2 appearance in the subset of the PDGFRα$^+$ population (red asterisk).
392 (*n = 3* independent experiments) (F) Representative IF imaging of 36 hours-cultured hiPSCs. (G)
393 Schematic summary of flow cytometry analysis. (H) qRT-PCR analyses further confirmed the
394 preceded *MIXL1* induction and subsequent expression of *PDGFRα* and *FOXA2*. All graphs: Data
395 normalized by undifferentiated iPSCs. Each plot showed a different biological experiment (n = 3
396 independent experiments).. Error bars represent mean ±SD.
397

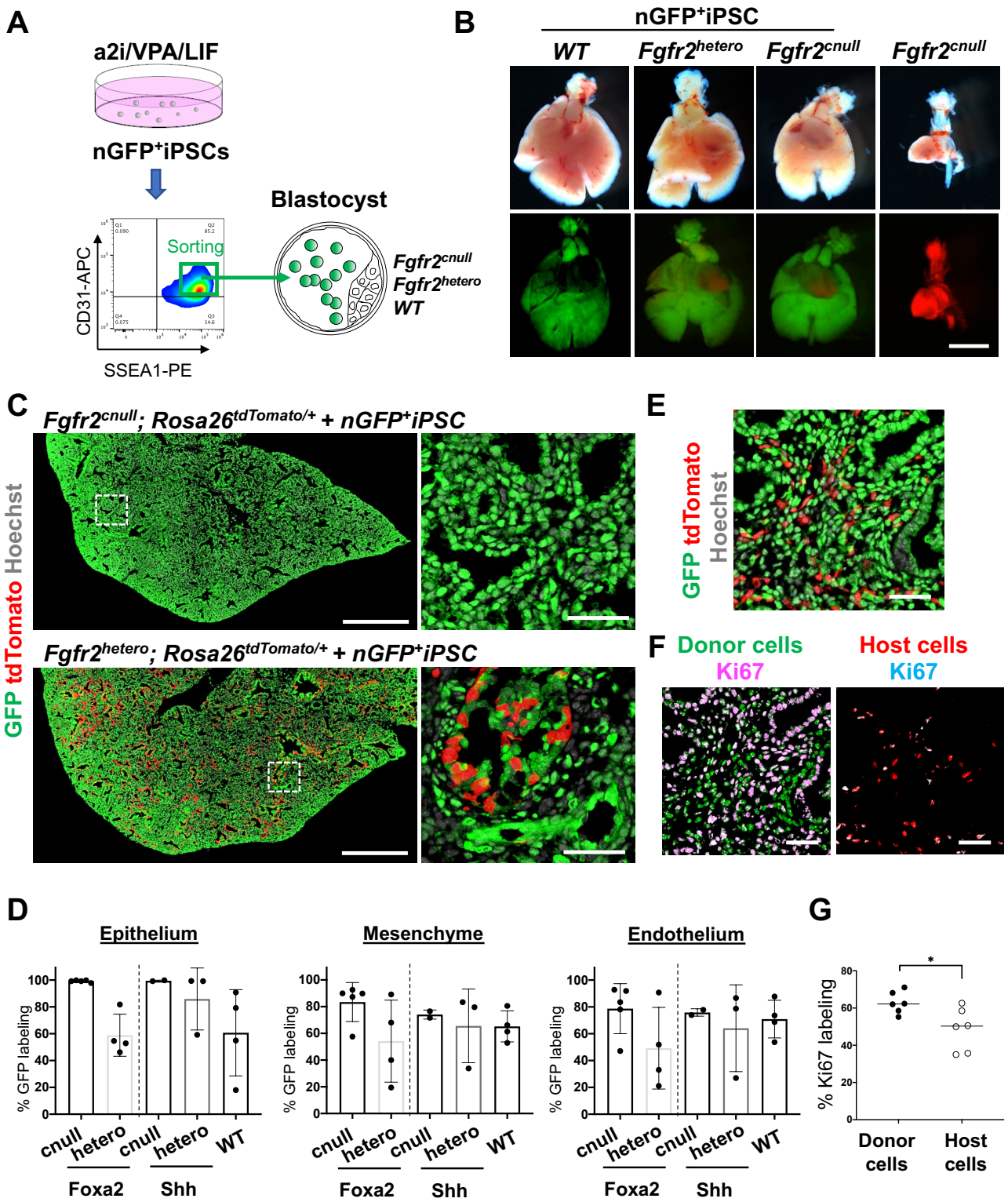

398

399 **Figure 4. Generation of the entire lungs in *Foxa2*-driven *Fgfr2*-deficient mice via CBC.**

400 (A) Schema of CBC experiment: a2i/VPA/LIF-treated SSEA1^{high} CD31^{high} nGFP^{+}iPSCs were
401 sorted and injected into WT, *Fgfr2*^{hetero} (heterozygous: *Foxa2*$^{cre/+}$*; Fgfr2*$^{flox/+}$*; Rosa26*$^{tdTomato/+}$), and
402 *Fgfr2*^{cnull} (homozygous: *Foxa2*$^{cre/+}$*; Fgfr2*$^{flox/flox}$*; Rosa26*$^{tdTomato/+}$) blastocysts. (B) Gross morphology,
403 GFP (green: donor nGFP^{+}iPSCs-derived signals), and tdTomato (host Foxa2-lineage-derived
404 signals) fluorescence of freshly isolated lungs from E17.5 chimeric *WT*(left), *Fgfr2*^{hetero} (left
405 middle), and *Fgfr2*^{cnull} (right middle) that were injected with nGFP^{+}iPSCs. Control: littermate
406 *Fgfr2*^{cnull} mouse without nGFP^{+}iPSCs injection (right). (C) IF-confocal imaging of E17.5 *Fgfr2*^{cnull}
407 or *Fgfr2*^{hetero} lungs injected with nGFP^{+}iPSCs. Dotted lines: enlarged images: Compared with
408 littermate control holding host-derived cells (red), E17.5 *Fgfr2*^{cnull} lungs were entirely composed
409 of donor-derived nGFP^{+} cells (green). (D) Graphs: % GFP in CD31^{-}Epcam^{+} lung epithelium,
410 CD31^{-}Epcam^{-} mesenchyme, and CD31^{+}Epcam^{-} endothelium analyzed by flow cytometry. Each
411 plot: a different biological animal. *Foxa2*$^{Cre/+}$*; Fgfr2*^{cnull}*; Rosa*^{tdTomato} (*n=5,* independent biological
412 replicates), *Foxa2*$^{Cre/+}$*; Fgfr2*^{hetero}*; Rosa*$^{tdTomato/+}$(*n=4*), *Shh*$^{Cre/+}$*; Fgfr2*^{cnull}*; Rosa*$^{tdTomato/+}$ (*n=2*),
413 *Shh*$^{Cre/+}$*; Fgfr2*^{hetero}*; Rosa*$^{tdTomato/+}$(*n=3*), and *WT* (*n=4*). (E and F) Representative IF staining of
414 E14.5 lung of *Fgfr2*^{cnull}. GFP and tdTomato indicate donor and host-derived cells, respectively. (E-
415 F) Residual tdTomato^{+} host cells in E14.5 *Foxa2*$^{Cre/+}$*; Fgfr2*^{cnull} chimeric lungs. (F) Split images of
416 (E) visualizing GFP^{+} donor cells and tdTomato^{+} host cells, co-stained with Ki67. (G) Graphs: %
417 Ki67 labeling in mesenchymal cells of E14.5 *Foxa2*$^{Cre/+}$*; Fgfr2*^{cnull} chimeric lungs. Statistical
418 analyses: paired Student's t-test, significance at $*P < 0.05$, ns: non-significant. Scale bars: B, C
419 (left, right), E, F =1mm, 500μm, 50μm, 20μm, 20μm.
420

421 **TABLES**

422 **Table. 1 E17.5 Chimerism of Foxa2 promoter-driven conditional blastocyst**

423 **complementation**

		Liver	Lung			
			Whole	Epithelium	Mesenchyme	Endothelium
Foxa2-Cre	*Fgfr2 cnull*	56.2	91.8	99.8	92.6	78.1
		54.8	90.6	99.2	90	92.8
		47.4	90.3	99.2	89.8	91.9
		38.5	87.7	99.8	87.3	83.5
		14	58.9	97.8	57.6	47.1
	Fgfr2 hetero	60.2	65.9	46.2	68.1	33.1
		56.3	88.8	81.8	89.2	90.7
		24.2	42.1	52.9	40	51.9
		9.16	22.7	54.6	19.4	21.1
Shh-Cre	*Fgfr2 cnull*	35.7	73.6	99.2	71.7	73.9
		13	79.2	99.8	76.5	77.8
	Fgfr2 hetero	57.4	83.1	99.3	79.6	86.6
		44.4	84.3	99.2	83.4	78.7
		13.8	35	59.2	33.8	27
	Wild type	56	68.5	79.2	66.2	73.6
		22.3	56.7	18	61.3	68.7
		20.1	53.1	54.9	52.9	53.7
		17	89.5	90.8	80.6	87.7

424

425

426 **Table. 2 E14.5 Chimerism of Foxa2 promoter-driven conditional blastocyst**

427 **complementation**

		Liver	Lung			
			Whole	Epithelium	Mesenchyme	Endothelium
Foxa2-Cre	***Fgfr2*** ^{cnull}	59.9	81.9	99.4	81.4	86.2
		51	75.4	99.4	75.4	56.8
		25.3	56.5	97.4	54.1	63.2
	Fgfr2 ^{hetero}	37.1	54.4	56.9	54	58.9
		29.8	48.6	83.3	47.7	47.3
		18.7	43.4	18	45	31
		0.54	0.24	0.91	0.1	2.11
		0.4	0.17	1.02	0.058	1.23
	Wild type	39	68.7	56.2	69.2	67.5
		29.4	81.1	62.7	81.8	80.8
		28.6	73.9	39.6	75.6	76.4
		13.8	29.5	5.57	30.4	29.6
		0	2.22	5.52	1.5	16

428

429

430 **Methods**

431 **Mouse.** *Shh*$^{Cre/+}$ mice (cat. 05622), *Rosa26*$^{tdTomato/\ tdTomato}$ mice (cat. 07914), Rosa26$^{nT\text{-}nG/nT\text{-}nG}$ mice
432 (cat. 023035) and *Pdgfrα*$^{CreERT2/+}$ mice (cat. 032770) were obtained from the Jackson Lab. X. Zhang
433 kindly gifted *Fgfr2*$^{flox/flox}$ mice. We further backcrossed these mice for over three generations with
434 CD-1 mice (cat. 022) from the Charles River. Dr. Nicole C Dubois kindly provided *Foxa2*$^{Cre/Cre}$
435 mice (129xB6 mixed background). For conditional deletion of *Fgfr2* (*Fgfr2*^{cnull}), we crossed
436 *Fgfr2*$^{flox/flox}$*; Rosa26*$^{tdTomato/tdTomato}$ females with *Foxa2*$^{Cre/Cre}$*; Fgfr2*$^{flox/+}$, *Foxa2*$^{Cre/+}$*; Fgfr2*$^{flox/+}$ or
437 *Shh*$^{Cre/+}$*; Fgfr2*$^{flox/+}$ males, respectively. PCR performed genotyping of the *Shh-Cre*, *Pdgfr α-*
438 *CreERT2*, *Rosa26-nTnG,* and *Rosa26-tdTomato* alleles according to the protocol provided by the
439 vendor. For the CBC, genotyping of chimeric animals was confirmed by GFP-negative sorted liver
440 cells and lung cells. For detecting the *Fgfr2* floxed allele, we performed PCR using the primer
441 sets: FR2-F1, 5′-ATAGGAGCAACAGGCGG-3′, and FR2-F2, 5′-CAAGAGGCGACCAGTCA-
442 3′(Mori et al., 2019). For lineage tracing with Pdgfrα$^{CreERT2/+}$; Rosa26$^{tdTomato/+}$ mice, 1 dose of 200
443 μg tamoxifen (MedChem Express, HY-13757A) per g of body weight was given via oral gavage
444 injection. All animal experiments were approved by Columbia University Institutional Animal
445 Care and Use Committee in accordance with US National Institutes of Health guidelines.

446

447 **Culture of mouse iPSC**. We cultured iPSC in a2i/VPA/LIF medium on a feeder, as previously
448 reported(Mori et al., 2019). These PSC cells were passaged at a split ratio of 1:10 every 2–3 d.

449

450 **Culture of human iPSCs (hiPSCs).** All iPSC lines were maintained in feeder-free conditions on
451 laminin iMatrix-511 silk E8 (Amsbio, AMS.892021) in StemFit 04 complete Medium (Amsbio,
452 SFB-504), supplemented with Primocin (Invivogen, ant-pm-1), and passaged with TrypLE Select

453 (Gibco, A1285901). All human iPSC lines used were characterized for pluripotency and were
454 found to be karyotypically normal. The BU3NGST cell line was kindly gifted by Dr. Finn Hawkins
455 and Dr. Darrell Kotton at Boston University, Boston, MA. Dr. Jennifer Davis, the University of
456 Washington School of Medicine, Seattle, WA, kindly gifted the Rainbow cell line. PD2 and TD1
457 hiPSC were generated from deidentified commercially available human peripheral blood
458 mononuclear cell and tracheal epithelial cell lines via the manufacturing protocol of Sendai virus-
459 mediated reprogramming (CytoTune2.0) (ThermoFisher, A16517). Every other month, all iPSC
460 lines screened negative for mycoplasma contamination using a MycoAlert PLUS detection kit
461 (Lonza, LT07-710).
462
463 **Differentiation of hiPSCs into lung epithelial and mesenchymal cells.** The directed
464 differentiation protocols were modified from previous protocols to maximize lung mesenchymal
465 cell generation concomitantly with NKX2-1^{+} lung epithelium. Briefly, DE and LPM precursors
466 were induced once seeded hiPSC-formed colonies by the Activin induction using the STEMdiff
467 Definitive Endoderm Kit (StemCell Technologies, 05110) for 72 hours. Differentiated cells were
468 dissociated and passaged in Laminin511-coated tissue culture plates in a complete serum-free
469 differentiation medium (cSFDM)(Chen et al., 2017). To induce DE and LPM into the anterior
470 foregut endoderm and mesoderm, the cSFDM was supplemented with 10μM SB431542
471 (MedChem Express, HY-10431) and 2μM Dorsomorphin (Tocris, 3093) for 48 hours and 10μM
472 SB431542 and 2μM IWP2 (Tocris, 3533) for 24 hours. Cells were then cultured for 7-10 additional
473 days in cSFDM containing 3μM CHIR99021, 10ng/ml recombinant human FGF10 (R&D Systems,
474 345-FG), 10ng/ml recombinant human KGF (R&D Systems, 251-KG), 10 ng/mL recombinant

475 human BMP4 (R&D Systems, 314-BP), and 50nM retinoid acid (Sigma-Aldrich, R2625) to induce
476 NKX2-1 positive lung epithelial cells and $WNT2^{+}TBX4^{+}$ lung mesenchymal cells.
477
478 **Immunofluorescence (IF).** Before the immunostaining, antigen retrieval was performed using
479 Unmasking Solution (Vector Laboratories, H-3300) for 10 min at around 100 °C by microwave.
480 7-μm tissue sections were incubated with primary antibodies in the buffer of M.O.M. kit (Vector
481 Laboratories, MKB-2213-1) overnight at 4 °C, washed in PBS, and incubated with secondary
482 antibodies conjugated with Alexa488, 567, or 647 (ThermoScientific, 1:400) with NucBlue Fixed
483 Cell Ready Probes Reagent (Hoechst) (ThermoScientific, R37605) for 1.5 h, and mounted with
484 ProLong Gold antifade reagent (Invitrogen, P36930). The images were captured by a Zeiss
485 confocal 710 microscopy. The antibodies were listed in the Supplemental Table. 1.
486
487 **Immunocytochemistry.** Cells on culture dishes were fixed with 4% Paraformaldehyde (PFA) for
488 30 min at room temperature (RT), permeabilized, and blocked with staining buffer containing
489 0.025% Triton X-100 and 1% BSA for 1 hour at RT. Primary antibodies (Supplementary Table 1)
490 were incubated overnight at 4 °C in the staining buffer. After three washes in PBS, secondary
491 antibodies (Supplementary Table 1) and NucBlue Fixed Cell Ready Probes Reagent (Hoechst)
492 were incubated for 1 h. The samples were imaged using DMi8 Leica widefield microscope. The
493 antibodies were listed in the Supplemental Table. 1.
494
495 **RNAScope in situ hybridization (ISH). RNA at** E18.5 lung sections were stained by RNAScope
496 probes: Mm-Foxa2-T8 (Advanced Cell Diagnostics, #409111-T8) or Negative control (NC)
497 (Advanced Cell Diagnostics, #324341) using the RNAScope HiPlex12 Reagent kit v2 (Advanced

498 Cell Diagnostics, #324419) according to manufacture-provided protocol. Then, sections were
499 incubated with tdTomato antibody for 2 hours at room temperature, washed in PBS, and incubated
500 with secondary antibody conjugated with Alexa488 with NucBlue Fixed Cell Ready Probes
501 Reagent (Hoechst) for 1.5 h, and mounted with ProLong Gold antifade reagent. The images of
502 *Foxa2* and NC ISH were captured with the same setting by a Zeiss confocal 710 microscopy.
503
504 **Flow cytometry (FCM) analyses of mouse lung tissue.** Lungs from lineage tracing mice at
505 E14.5, E18.5, P0, four weeks or lungs from CBC chimeric mice at E14.5 and E17.5 were harvested
506 and prepared for the FCM, as previously described(Mori et al., 2019). Briefly, tissues were minced
507 with microscissors, and 1 ml of pre-warmed dissociation buffer (1 mg/ml DNase (Sigma, DN25),
508 5 mg/ml collagen (Roche, 10103578001), and 15 U/ml Dispase II (Stemcell Technologies, 7913)
509 in HBSS), incubated at 37 °C on the rocker with 50 r.p.m. speed, and neutralized with the
510 dissociation buffer by FACS buffer containing 2% FBS, Glutamax, 2mM EDTA and 10mM
511 HEPES in HBSS after the 30 min incubation. After filtrating the cells with a 40-μm filter
512 (FALCON, 352235), cell pellets were resuspended with 1 ml of cold RBC lysis buffer (Biolegend,
513 420301) to lyse the remaining erythrocytes for 5 min on ice, and neutralized by 1 ml cold FACS
514 buffer. After that, it was centrifuged them at 350 rcf, 4 °C, for 3 min to remove the lysed blood
515 cells. For FCM analysis, one million cells were transferred in 100 μl of FACS buffer supplemented
516 with 0.5μM Y27632 and then added 2 μl Fc Block (BD Pharmingen, 553141) per sample followed
517 by 10 min incubation on ice. Cells were incubated with the following antibodies: CD31-APC
518 (Biolegend, 102510, 1/50), Epcam-BV711 (BioLegend, 118233, 1/50), or Epcam-BV421
519 (Biolegend, 118225, 1/50), Aqua Zombie (BioLegend, 423101, 1/100), CD45-BV605
520 (BioLegend, 103104, 1/50) for 30 min on ice. After staining, cells were washed twice with FACS

521 buffer before resuspending in 500 μl FACS buffer for the subsequent analyses using SONY
522 MA900 or NovoCyte. Compensation was manually performed to minimize the tdTomato signal
523 leakage to the GFP channel using FlowJo (ver. 10. 7. 1). 2 samples from E14.5 lineage tracing
524 mice were removed from analysis based on inaccurate staining of live staining. Total 4 lungs were
525 calculated from 6 embryos.
526
527 **nGFP$^+$iPSC establishment and preparation for CBC donor.**
528 E14.5 lung tissues of *Rosa26$^{nTnG/nTnG}$* mice (JAX, cat. 023035, C57BL/6NJ background) were
529 harvested in a dissociation buffer described above. The dissociated cells were seeded on a 10cm
530 dish, and only lung fibroblast survived after 1 week in MEF medium(Mori et al., 2019). The
531 fibroblasts were passaged using Accutase (Innovative Cell Technologies, AT104) and seeded on
532 gelatin (Millipore-Sigma, ES006B)-coated 6-well plates with a density of 0.1 million cells per
533 well. Upon cell attachment, Yamanaka reprogramming factors were induced to iPSCs via Sendai
534 virus using CytoTune2.0 (ThermoFisher, A16517). To establish nGFP$^+$ iPSCs, the Cre plasmid
535 was transfected using Fugene HD transfection reagent (Promega, E2311), then sorted out
536 GFP$^+$tdTomato$^-$ live cells by FACS (SONYMA900), and single clones were expanded.
537 For the CBC donor cell preparation, nGFP$^+$iPSCs cultured in a2i/VPA/LIF(Mori et al., 2019) were
538 trypsinized and resuspended in 4 ml cold DMEM + 10% FBS immediately and filtering the cells
539 with a 40-μm filter. Cells were centrifuged at 350 rcf, 4 °C, for 3 min, and the supernatant was
540 removed. After being washed with flow buffer containing 0.2% BSA, 1% Glutamax, and 1μM
541 Y27632, the cells were resuspended in 100μl/1 million cells with flow buffer. The following
542 antibodies were added: Epcam-BV421 (1:50), SSEA1-PE (1:50), CD31-APC (1:50), Zombie

543 Aqua Fixable Viability Kit (1:100). Epcam^{high}SSEA1^{high}CD31^{high} cells were sorted by FACS
544 (SONYMA900) and subsequently prepared for the injection.
545
546 **Blastocyst preparation and embryo transfer.** Blastocysts were prepared by mating *Foxa2*$^{Cre/Cre}$;
547 *Fgfr2*$^{flox/+}$,*Foxa2*$^{Cre/+}$; *Fgfr2*$^{flox/+}$ or *Shh*$^{Cre/+}$; *Fgfr2*$^{flox/+}$ males (all 129 x B6 x CD-1 background) with
548 superovulated Fgfr2$^{flox/flox}$; Rosa26$^{tdTomato/tdTomato}$ females (129 x B6 x CD-1 background). Blastocysts
549 were harvested at E3.5 after superovulation(Mori et al., 2019). 20 sorted nGFP^{+}iPSCs were
550 injected into each blastocyst. After the iPSC injection, blastocysts were cultured in an M2 medium
551 (Cosmobio) for a few hours in a 37 °C, 5% CO2 incubator for recovery. Then, blastocysts were
552 transferred to the uterus of the pseudopregnant foster mother.
553
554 **Real-time-quantitative RT-PCR (qRT-PCR).** Total RNA was extracted using a Direct-zol™
555 RNA MiniPrep Plus kit (Zymo Research, R2072), and cDNA was synthesized using Primescript™
556 RT Master Mix (Takara, RR036B). The cDNAs were then used as templates for qRT-PCR analysis
557 with gene-specific primers. Reactions (10 μl) were performed Luna® Universal qPCR Master Mix
558 (New England Biolabs, M3003X). mRNA abundance for each gene was determined relative to
559 GAPDH mRNA using the $2^{-\Delta\Delta Ct}$ method. The primers were listed in the Supplemental Table. 2.
560 Data were represented as mean ± SD of measurements. The number of animals or cells per group
561 is provided in the legends. The undetected values in each biological experiment in Fig.3d were
562 removed from the graphs.
563
564 **Statistical analysis.** Data analysis was performed using Prism 8. Data acquired by performing
565 biological replicas of two or three independent experiments are presented as the mean ± SD.

566 Statistical significance was determined using a two-tailed t-test and unpaired one-way or two-way
567 ANOVA with the Tukey post hoc test. *$P < 0.05$, **$P < 0.01$, ***$P < 0.001$, ns: non-significant.
568
569 **Data availability.** scRNA-seq data for mouse gastrulation and early organogenesis described in
570 the manuscript have been analyzed from the deposited database at
571 https://marionilab.cruk.cam.ac.uk/MouseGastrulation2018/. The authors declare that all data
572 supporting the results of this study are available within the paper and the Supplementary
573 Information. Raw data are available from the corresponding author upon reasonable request.
574
575 **References**

576 Arman E, Haffner-Krausz R, Gorivodsky M, Lonai P. 1999. Fgfr2 is required for limb outgrowth
577 and lung-branching morphogenesis. *Proceedings of the National Academy of Sciences*
578 **96**:11895–11899. doi:10.1073/pnas.96.21.11895
579 Artus J, Panthier JJ, Hadjantonakis AK. 2010. A role for PDGF signaling in expansion of the
580 extra-embryonic endoderm lineage of the mouse blastocyst. *Development* **137**:3361–3372.
581 doi:10.1242/dev.050864
582 Bardot E, Calderon D, Santoriello F, Han S, Cheung K, Jadhav B, Burtscher I, Artap S, Jain R,
583 Epstein J, Lickert H, Gouon-Evans V, Sharp AJ, Dubois NC. 2017. Foxa2 identifies a
584 cardiac progenitor population with ventricular differentiation potential. *Nat Commun* **8**:1–
585 15. doi:10.1038/ncomms14428
586 Cardoso W v, Kotton DN. 2008. Specification and patterning of the respiratory system.
587 *Stembook* 1–18. doi:10.3824/stembook.1.10.1

588 Chen J, Lansford R, Stewart V, Young F, Alt FW. 1993. RAG-2-deficient blastocyst
589 complementation: an assay of gene function in lymphocyte development. *Proceedings of*
590 *the National Academy of Sciences* **90**:4528–4532. doi:10.1073/pnas.90.10.4528
591 Chen Y-W, Huang SX, de Carvalho ALRT, Ho S-H, Islam MN, Volpi S, Notarangelo LD,
592 Ciancanelli M, Casanova J-L, Bhattacharya J, Liang AF, Palermo LM, Porotto M, Moscona
593 A, Snoeck H-W. 2017. A three-dimensional model of human lung development and disease
594 from pluripotent stem cells. *Nat Cell Biol* **19**:542–549. doi:10.1038/ncb3510
595 Christodoulou C, Longmire TA, Shen SS, Bourdon A, Sommer CA, Gadue P, Spira A, Gouon-
596 Evans V, Murphy GJ, Mostoslavsky G, Kotton DN. 2011. Mouse ES and iPS cells can form
597 similar definitive endoderm despite differences in imprinted genes. *Journal of Clinical*
598 *Investigation* **121**:2313–2325. doi:10.1172/JCI43853
599 Crapo JD, Barry BE, Gehr P, Bachofen M, Weibel ER. 1982. Cell number and cell
600 characteristics of the normal human lung. *American Review of Respiratory Disease*
601 **126**:332–337. doi:10.1164/arrd.1982.126.2.332
602 De Langhe SP, Carraro G, Warburton D, Hajihosseini MK, Bellusci S. 2006. Levels of
603 mesenchymal FGFR2 signaling modulate smooth muscle progenitor cell commitment in the
604 lung. *Dev Biol* **299**:52–62. doi:10.1016/j.ydbio.2006.07.001
605 De Moerlooze L, Spencer-Dene B, Revest JM, Hajihosseini M, Rosewell I, Dickson C. 2000. An
606 important role for the IIIb isoform of fibroblast growth factor receptor 2 (FGFR2) in
607 mesenchymal-epithelial signalling during mouse organogenesis. *Development* **127**:483–92.
608 Devine WP, Wythe JD, George M, Koshiba-Takeuchi K, Bruneau BG. 2014. Early patterning
609 and specification of cardiac progenitors in gastrulating mesoderm. *Elife* **3**.
610 doi:10.7554/ELIFE.03848

611 Gotoh S, Ito I, Nagasaki T, Yamamoto Y, Konishi S, Korogi Y, Matsumoto H, Muro S, Hirai T,
612 Funato M, Mae SI, Toyoda T, Sato-Otsubo A, Ogawa S, Osafune K, Mishima M. 2014.
613 Generation of alveolar epithelial spheroids via isolated progenitor cells from human
614 pluripotent stem cells. *Stem Cell Reports* **3**:394–403. doi:10.1016/j.stemcr.2014.07.005
615 Green MD, Chen A, Nostro M-C, d'Souza SL, Schaniel C, Lemischka IR, Gouon-Evans V,
616 Keller G, Snoeck H-W. 2011. Generation of anterior foregut endoderm from human
617 embryonic and induced pluripotent stem cells. *Nat Biotechnol* **29**:267–72.
618 doi:10.1038/nbt.1788
619 Guyette JP, Gilpin SE, Charest JM, Tapias LF, Ren X, Ott HC. 2014. Perfusion decellularization
620 of whole organs. *Nat Protoc* **9**:1451–68. doi:10.1038/nprot.2014.097
621 Hackett TL, Knight D a, Sin DD. 2010. Potential role of stem cells in management of COPD. *Int*
622 *J Chron Obstruct Pulmon Dis* **5**:81–8.
623 Hamanaka S, Umino A, Sato H, Hayama T, Yanagida A, Mizuno N, Kobayashi T, Kasai M,
624 Suchy FP, Yamazaki S, Masaki H, Yamaguchi T, Nakauchi H. 2018. Generation of
625 Vascular Endothelial Cells and Hematopoietic Cells by Blastocyst Complementation. *Stem*
626 *Cell Reports* **11**:988–997. doi:10.1016/j.stemcr.2018.08.015
627 Han L, Chaturvedi P, Kishimoto K, Koike H, Nasr T, Iwasawa K, Giesbrecht K, Witcher PC,
628 Eicher A, Haines L, Lee Y, Shannon JM, Morimoto M, Wells JM, Takebe T, Zorn AM.
629 2020. Single cell transcriptomics identifies a signaling network coordinating endoderm and
630 mesoderm diversification during foregut organogenesis. *Nat Commun* **11**.
631 doi:10.1038/s41467-020-17968-x

632 Harris KS, Zhang Z, McManus MT, Harfe BD, Sun X. 2006. Dicer function is essential for lung
633 epithelium morphogenesis. *Proc Natl Acad Sci U S A* **103**:2208–13.
634 doi:10.1073/pnas.0510839103
635 Hart AH, Hartley L, Sourris K, Stadler ES, Li R, Stanley EG, Tam PPL, Elefanty AG, Robb L.
636 2002. Mixl1 is required for axial mesendoderm morphogenesis and patterning in the murine
637 embryo. *Development* **129**:3597–608.
638 Hawkins F, Kramer P, Jacob A, Driver I, Thomas DC, Mccauley KB, Skvir N, Crane AM,
639 Kurmann AA, Hollenberg AN, Nguyen S, Wong BG, Khalil AS, Huang SXL, Guttentag S,
640 Rock JR, Shannon JM, Davis BR, Kotton DN. 2017. Prospective isolation of NKX2-1 –
641 expressing human lung progenitors derived from pluripotent stem cells. *J Clin Invest* **127**:1–
642 18. doi:10.1172/JCI89950
643 Horn S, Kobberup S, Jørgensen MC, Kalisz M, Klein T, Kageyama R, Gegg M, Lickert H,
644 Lindner J, Magnuson MA, Kong YY, Serup P, Ahnfelt-Rønne J, Jensen JN. 2012. Mind
645 bomb 1 is required for pancreatic β-cell formation. *Proc Natl Acad Sci U S A* **109**:7356–
646 7361. doi:10.1073/pnas.1203605109
647 Huang SXL, Islam MN, O'Neill J, Hu Z, Yang Y-G, Chen Y-W, Mumau M, Green MD,
648 Vunjak-Novakovic G, Bhattacharya J, Snoeck H-W. 2014. Efficient generation of lung and
649 airway epithelial cells from human pluripotent stem cells. *Nat Biotechnol* **32**:84–91.
650 doi:10.1038/nbt.2754
651 Kadzik RS, Morrisey EE. 2012. Directing lung endoderm differentiation in pluripotent stem
652 cells. *Cell Stem Cell* **10**:355–61. doi:10.1016/j.stem.2012.03.013

653 Kemter E, Schnieke A, Fischer K, Cowan PJ, Wolf E. 2020. Xeno-organ donor pigs with
654 multiple genetic modifications - the more the better? *Curr Opin Genet Dev* **64**:60–65.
655 doi:10.1016/J.GDE.2020.05.034
656 Kitahara A, Ran Q, Oda K, Yasue A, Abe M, Ye X, Sasaoka T, Tsuchida M, Sakimura K,
657 Ajioka Y, Saijo Y, Zhou Q. 2020. Generation of Lungs by Blastocyst Complementation in
658 Apneumic Fgf10-Deficient Mice. *Cell Rep* **31**:107626.
659 doi:10.1016/J.CELREP.2020.107626
660 Kobayashi T, Yamaguchi T, Hamanaka S, Kato-Itoh M, Yamazaki Y, Ibata M, Sato H, Lee Y-S,
661 Usui J-I, Knisely a S, Hirabayashi M, Nakauchi H. 2010. Generation of rat pancreas in
662 mouse by interspecific blastocyst injection of pluripotent stem cells. *Cell* **142**:787–99.
663 doi:10.1016/j.cell.2010.07.039
664 Konishi S, Gotoh S, Tateishi K, Yamamoto Y, Korogi Y, Nagasaki T, Matsumoto H, Muro S,
665 Hirai T, Ito I, Tsukita S, Mishima M. 2016. Directed Induction of Functional Multi-ciliated
666 Cells in Proximal Airway Epithelial Spheroids from Human Pluripotent Stem Cells. *Stem*
667 *Cell Reports* **6**:18–25. doi:10.1016/j.stemcr.2015.11.010
668 Kopper O, Benvenisty N. 2012. Stepwise differentiation of human embryonic stem cells into
669 early endoderm derivatives and their molecular characterization. *Stem Cell Res* **8**:335–345.
670 doi:10.1016/j.scr.2011.12.006
671 Kotton DN, Morrisey EE. 2014. Lung regeneration: Mechanisms, applications and emerging
672 stem cell populations. *Nat Med* **20**:822–832. doi:10.1038/nm.3642
673 Li E, Ustiyan V, Wen B, Kalin GT, Whitsett JA, Kalin T v., Kalinichenko V v. 2021. Blastocyst
674 complementation reveals that NKX2-1 establishes the proximal-peripheral boundary of the
675 airway epithelium. *Dev Dyn* **250**:1001–1020. doi:10.1002/DVDY.298

676 Mori M, Furuhashi K, Danielsson JA, Hirata Y, Kakiuchi M, Lin CS, Ohta M, Riccio P,
677 Takahashi Y, Xu X, Emala CW, Lu C, Nakauchi H, Cardoso W v. 2019. Generation of
678 functional lungs via conditional blastocyst complementation using pluripotent stem cells.
679 *Nat Med* **25**:1691–1698. doi:10.1038/s41591-019-0635-8
680 Ng WH, Johnston EK, Tan JJ, Bliley JM, Feinberg AW, Stolz DB, Sun M, Wijesekara P,
681 Hawkins F, Kotton DN, Ren X. 2022. Recapitulating Human Cardio-pulmonary Co-
682 development Using Simultaneous Multilineage Differentiation of Pluripotent Stem Cells.
683 *Elife* **11**:1–27. doi:10.7554/eLife.67872
684 Ott HC, Clippinger B, Conrad C, Schuetz C, Pomerantseva I, Ikonomou L, Kotton D, Vacanti
685 JP. 2010. Regeneration and orthotopic transplantation of a bioartificial lung. *Nat Med*
686 **16**:927–33. doi:10.1038/nm.2193
687 Peng T, Tian Y, Boogerd CJ, Lu MM, Kadzik RS, Stewart KM, Evans SM, Morrisey EE. 2013.
688 Coordination of heart and lung co-development by a multipotent cardiopulmonary
689 progenitor. *Nature* **500**:589–592. doi:10.1038/nature12358
690 Petersen TH, Calle EA, Zhao L, Lee EJ, Gui L, Raredon MSB, Gavrilov K, Yi T, Zhuang ZW,
691 Breuer C, Herzog E, Niklason LE. 2010. Tissue-engineered lungs for in vivo implantation.
692 *Science (1979)* **329**:538–541. doi:10.1126/science.1189345
693 Pijuan-Sala B, Griffiths JA, Guibentif C, Hiscock TW, Jawaid W, Calero-Nieto FJ, Mulas C,
694 Ibarra-Soria X, Tyser RCV, Ho DLL, Reik W, Srinivas S, Simons BD, Nichols J, Marioni
695 JC, Göttgens B. 2019. A single-cell molecular map of mouse gastrulation and early
696 organogenesis. *Nature* **566**:490–495. doi:10.1038/s41586-019-0933-9
697 Scheibner K, Schirge S, Burtscher I, Büttner M, Sterr M, Yang D, Böttcher A, Ansarullah, Irmler
698 M, Beckers J, Cernilogar FM, Schotta G, Theis FJ, Lickert H. 2021. Epithelial cell plasticity

699 drives endoderm formation during gastrulation. *Nat Cell Biol* **23**:692–703.
700 doi:10.1038/s41556-021-00694-x
701 Sekine K, Ohuchi H, Fujiwara M, Yamasaki M, Yoshizawa T, Sato T, Yagishita N, Matsui D,
702 Koga Y, Itoh N, Kato S. 1999. Fgf10 is essential for limb and lung formation. *Nat Genet*
703 **21**:138–41. doi:10.1038/5096
704 Stone KC, Mercer RR, Gehr P, Stockstill B, Crapo JD. 1992. Allometric Relationships of Cell
705 Numbers and Size in the Mammalian Lung. *Am J Respir Cell Mol BioI* **6**:235–243.
706 Tada S, Era T, Furusawa C, Sakurai H, Nishikawa S, Kinoshita M, Nakao K, Chiba T,
707 Nishikawa SI. 2005. Characterization of mesendoderm: A diverging point of the definitive
708 endoderm and mesoderm in embryonic stem cell differentiation culture. *Development*
709 **132**:4363–4374. doi:10.1242/dev.02005
710 Tian L, Gao J, Garcia IM, Chen HJ, Castaldi A, Chen YW. 2021. Human pluripotent stem cell-
711 derived lung organoids: Potential applications in development and disease modeling. *Wiley*
712 *Interdiscip Rev Dev Biol* **10**:1–16. doi:10.1002/wdev.399
713 Tian Y, Zhang Y, Hurd L, Hannenhalli S, Liu F, Lu MM, Morrisey EE. 2011. Regulation of lung
714 endoderm progenitor cell behavior by miR302/367. *Development* **138**:1235–45.
715 doi:10.1242/dev.061762
716 Travaglini KJ, Nabhan AN, Penland L, Sinha R, Gillich A, Sit R v., Chang S, Conley SD, Mori
717 Y, Seita J, Berry GJ, Shrager JB, Metzger RJ, Kuo CS, Neff N, Weissman IL, Quake SR,
718 Krasnow MA. 2020. A molecular cell atlas of the human lung from single-cell RNA
719 sequencing. *Nature* **587**:619–625. doi:10.1038/s41586-020-2922-4

720 Usui J, Kobayashi T, Yamaguchi T, Knisely a S, Nishinakamura R, Nakauchi H. 2012.
721 Generation of kidney from pluripotent stem cells via blastocyst complementation. *Am J*
722 *Pathol* **180**:2417–26. doi:10.1016/j.ajpath.2012.03.007
723 Wan H, Kaestner KH, Ang SL, Ikegami M, Finkelman FD, Stahlman MT, Fulkerson PC,
724 Rothenberg ME, Whitsett JA. 2004. Foxa2 regulates alveolarization and goblet cell
725 hyperplasia. *Development* **131**:953–964. doi:10.1242/dev.00966
726 Wang X. 2019. Bioartificial Organ Manufacturing Technologies. *Cell Transplant* **28**:5–17.
727 doi:10.1177/0963689718809918
728 Weaver M, Yingling JM, Dunn NR, Bellusci S, Hogan BL. 1999. Bmp signaling regulates
729 proximal-distal differentiation of endoderm in mouse lung development. *Development*
730 **126**:4005–4015.
731 Wen B, Li E, Ustiyan V, Wang G, Guo M, Na CL, Kalin GT, Galvan V, Xu Y, Weaver TE,
732 Kalin T v., Whitsett JA, Kalinichenko V v. 2021. In vivo generation of lung and thyroid
733 tissues from embryonic stem cells using blastocyst complementation. *Am J Respir Crit Care*
734 *Med* **203**:471–483. doi:10.1164/RCCM.201909-
735 1836OC/SUPPL_FILE/DISCLOSURES.PDF
736 Xing Y, Li C, Hu L, Tiozzo C, Li M, Chai Y, Bellusci S, Anderson S, Minoo P. 2008.
737 Mechanisms of TGFbeta inhibition of LUNG endodermal morphogenesis: the role of
738 TbetaRII, Smads, Nkx2.1 and Pten. *Dev Biol* **320**:340–50. doi:10.1016/j.ydbio.2008.04.044
739 Yamaguchi T, Sato H, Kato-Itoh M, Goto T, Hara H, Sanbo M, Mizuno N, Kobayashi T,
740 Yanagida A, Umino A, Ota Y, Hamanaka S, Masaki H, Rashid ST, Hirabayashi M,
741 Nakauchi H. 2017. Interspecies organogenesis generates autologous functional islets.
742 *Nature* **542**:191–196. doi:10.1038/nature21070

743 SUPPLEMENTAL FIGURES.

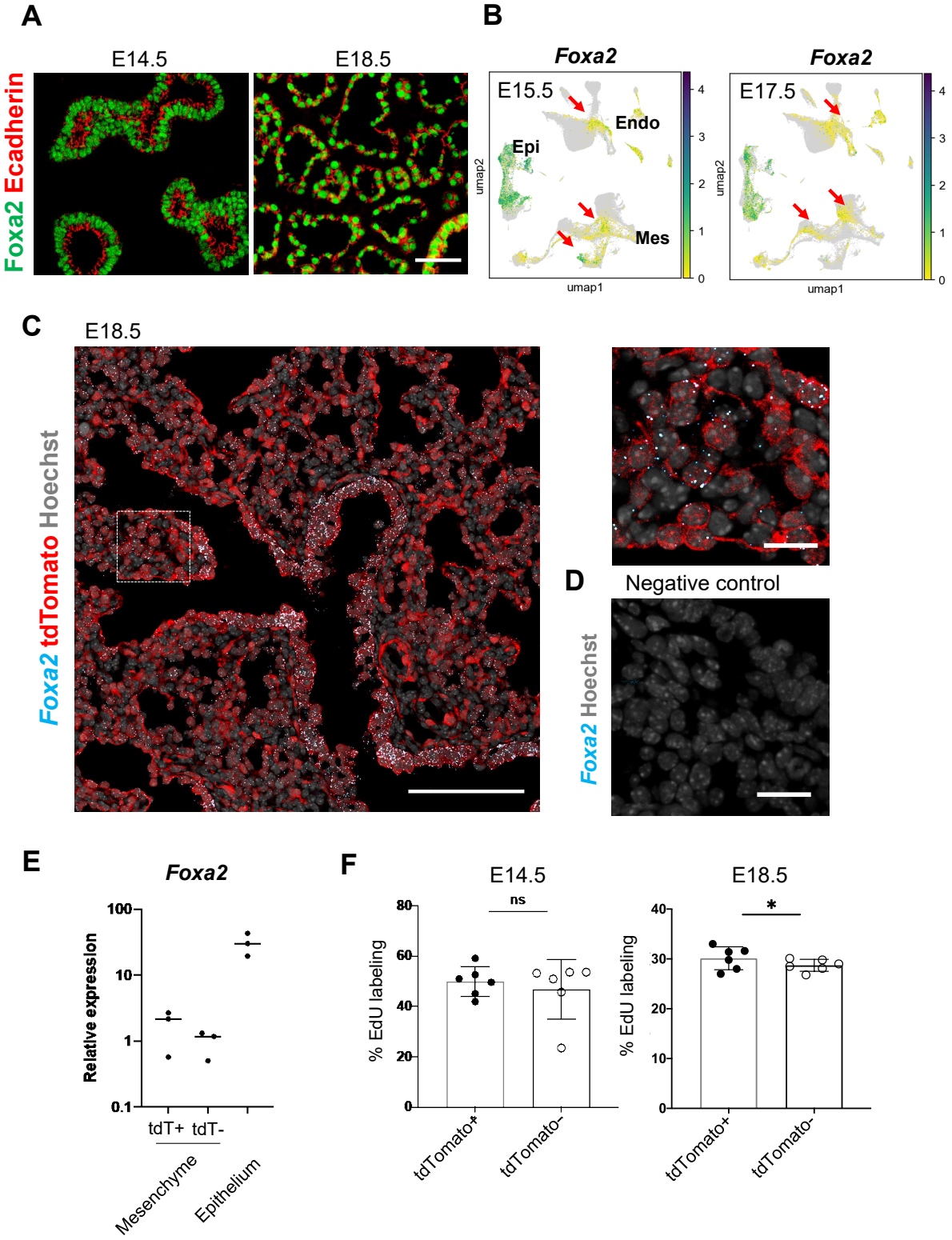

744

745 **Figure S1. Foxa2-lineage gradually increased in the mesenchyme and endothelial cells during**
746 **mouse lung development.** (A) Representative IF-confocal imaging of E14.5 and E18.5 mouse
747 embryonic lungs. Foxa2 (green) was expressed in lung epithelial cells labeled by E-cadherin (red)
748 but not in E-cadherin negative lung mesenchymal area. Scale bar = 50μm (B) Single-cell analysis
749 of mouse LungMAP. *Foxa2* expression was observed in lung mesenchyme and endothelium in
750 E15.5 and E17.5 (Arrows). (C), (D) Representative IF and in situ hybridization-confocal imaging
751 of E18.5 mouse embryonic lungs. Dotted lines: enlarged image. *Foxa2* mRNA was expressed in
752 lung epithelial cells and lung mesenchyme. Most of the *Foxa2* mRNA expression was colocalized
753 with tdTomato. Scale bars (left, right) = 50 μm, 20μm (E) Graphs: *Foxa2* qPCR for tdTomato
754 $(tdT)^{+}$ or $tdTomato^{-}$ $CD45^{-}$ $CD31^{-}$ $EPCAM^{-}$ mesenchymal cells and $CD45^{-}CD31^{-}EpCAM^{+}$
755 epithelial cells sorted by FACS from E18.5 Foxa2-lineage tracing mice. (n = 3, each biological
756 replicate) (F) Flow cytometry quantitative analyses: EdU labeling cells in $CD31^{+}Epcam^{-}$
757 endothelium at E14.5 and E18.5 (n = 6 each independent biological replicates, respectively) of
758 $Foxa2^{Cre/+}$; $Rosa^{tdTomato/+}$ lungs. Statistical analysis: paired Student's t-test, significance at $*P < 0.05$,
759 ns: non-significant.
760

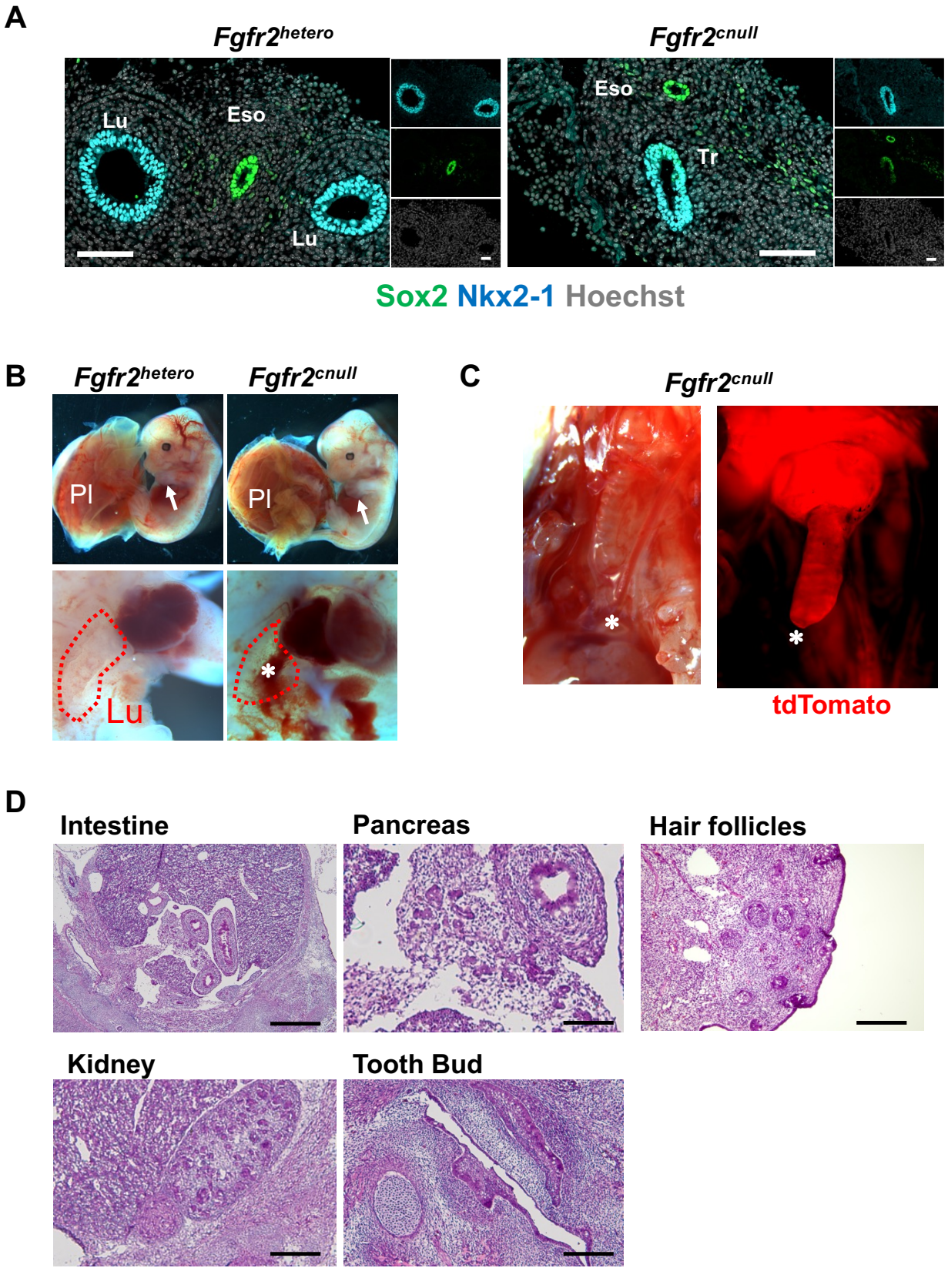
A
Fgfr2hetero
Fgfr2cnull
Lu
Eso
Lu
Eso
Tr
Sox2 Nkx2-1 Hoechst
B
Fgfr2hetero
Fgfr2cnull
Pl
Pl
Lu
C
Fgfr2cnull
tdTomato
D
Intestine
Pancreas
Hair follicles
Kidney
Tooth Bud

761

762 **Figure S2. Lung agenesis phenotype in the *Foxa2$^{Cre/+}$Fgfr2^{cnull}* mice.**

763 (A) Representative IF staining of E10.5 *Foxa2$^{Cre/+}$;Fgfr2^{hetero}* and *Foxa2$^{Cre/+}$;Fgfr2^{cnull}*: *Fgfr2^{cnull}* did
764 not form Sox2^{+}NKX2-1^{+}proximal airway bifurcation. Scale bar = 200μm. Lu: lung, Eso:
765 Esophagus. Tr: trachea. Nkx2-1 (blue), Sox2 (green). (B) Representative Gross morphology of
766 E14.5 *Foxa2$^{Cre/+}$;Fgfr2^{hetero}* and *Foxa2$^{Cre/+}$;Fgfr2^{cnull}*: No difference in the appearance of the embryo
767 between *Fgfr2^{hetero}* and *Fgfr2^{cnull}* (Top). Limb (arrows) and placenta (pl) are present in mice of all
768 genotypes. Conversely, the *Fgfr2^{cnull}* embryo showed lung agenesis phenotype (Bottom, asterisk)
769 (n = 6 per each group). (C) Representative image of *Fgfr2^{cnull}* lungs. Foxa2 lineage^{+} tdTomato
770 signal indicates the trachea ends in the middle of the thoracic cavity (asterisk). (D) HE staining:
771 The internal organs such as the intestine, pancreas, kidney, tooth buds, and hair follicles were
772 normally formed in *Fgfr2^{cnull}* E16.5 embryos. Scale bar = 500μm.

773

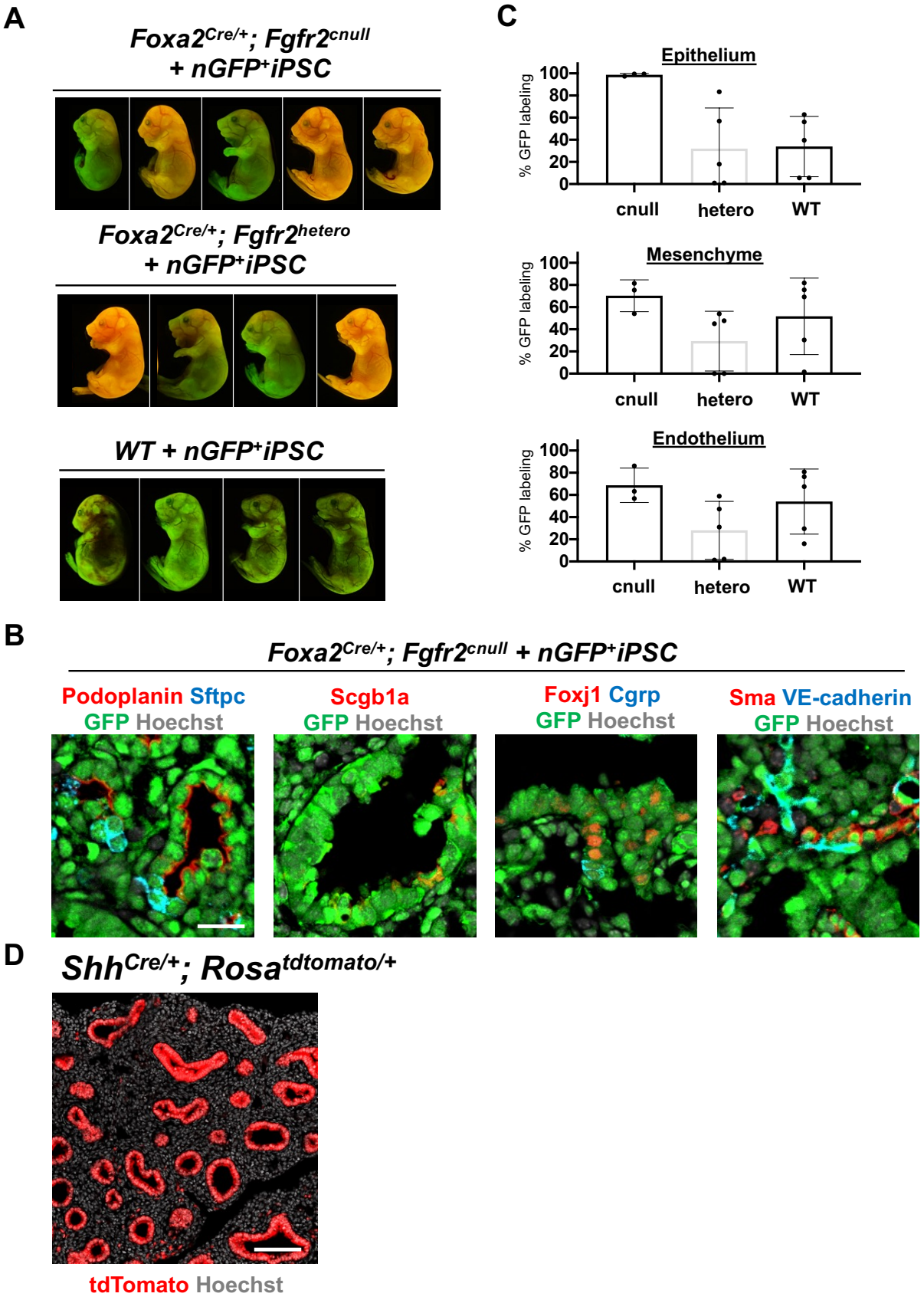
A
Foxa2Cre/+; Fgfr2cnull
+ nGFP+iPSC
Foxa2Cre/+; Fgfr2hetero
+ nGFP+iPSC
WT + nGFP+iPSC
C
Epithelium
Mesenchyme
Endothelium
% GFP labeling
100
80
60
40
20
0
cnull
hetero
WT
B
Foxa2Cre/+; Fgfr2cnull + nGFP+iPSC
Podoplanin Sftpc
GFP Hoechst
Scgb1a
GFP Hoechst
Foxj1 Cgrp
GFP Hoechst
Sma VE-cadherin
GFP Hoechst
D
ShhCre/+; RosatdtomatoO/+
tdTomato Hoechst

774

775 **Figure S3. The complemented embryos of *Foxa2*$^{Cre/+}$; *Fgfr2*^{cnull} +nGFP^{+}iPSCs showed**
776 **normal gross morphology and various chimerism** (A) Representative gross morphology of
777 chimeric embryos of *WT* + nGFP^{+}iPSCs, *Foxa2*$^{Cre/+}$; *Fgfr2*^{hetero} + nGFP^{+}iPSCs, *Foxa2*$^{Cre/+}$;
778 *Fgfr2*^{cnull} +nGFP^{+}iPSCs. The color indicated various GFP^{+} chimerism on the skin of those
779 embryos and the residual host Foxa2- lineage^{+} tdTomato signals. (B) Representative IF-confocal
780 imaging of E17.5 lungs of chimeric *Fgfr2*^{cnull}+ nGFP^{+}iPSCs. The E17.5 rescued lungs from
781 *Fgfr2*^{cnull} +nGFP^{+}iPSCs expressed differentiated cell markers such as Podoplanin (alveolar type1
782 cells), Sftpc (type 2 cells), Scg1a1 (club cells), Foxj1 (multiciliated cells), Cgrp (neuroendocrine
783 cells), Sma (smooth muscle cells), and VE-cadherin (endothelial cells). Scale bar = 20μm. (C)
784 Graphs: % of donor cell chimerism: % of GFP in CD31^{-}Epcam^{+} lung epithelium fraction, CD31^{-}
785 Epcam^{-} mesenchyme, and CD31^{+}Epcam^{-} endothelium analyzed by flow cytometry. Each plot: a
786 different biological animal (see table 2). *Foxa2*$^{Cre/+}$; *Fgfr2*^{cnull}; *Rosa*^{tdTomato} (*n=3,* independent
787 biological replicates), *Foxa2*$^{Cre/+}$; *Fgfr2*^{hetero}; *Rosa*$^{tdTomato/+}$(*n=5*), and *WT* (*n=5*) at E14.5. (D)
788 Representative IF-confocal imaging of E14.5 Shh-lineage tracing mouse lungs (*Shh*$^{Cre/+}$;
789 *Rosa*$^{tdTomato/+}$). Shh-lineage labeled the entire lung epithelium but rarely mesenchyme, distinct
790 from Foxa2 lineage mice (see Fig. 2F). Scale bar = 100μm.
791

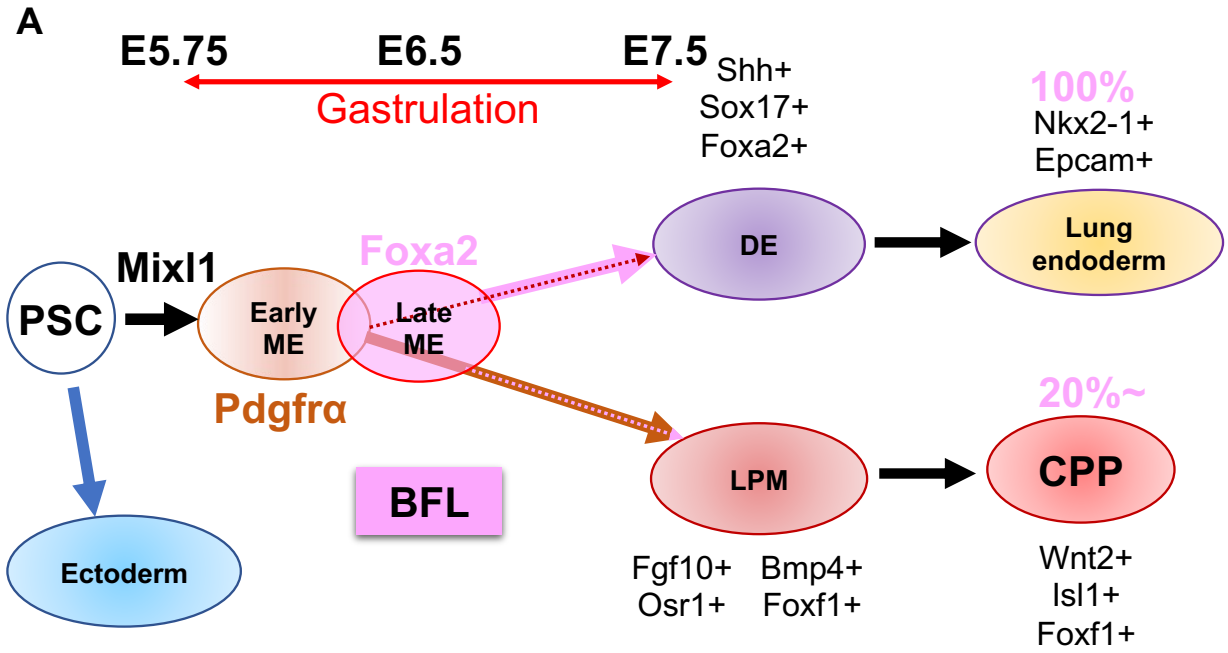

ME*: mesendoderm (primitive streak ~ nascent mesoderm)

Foxa2 lineage ⇨ All lung epithelium & part of the lung mesenchyme
Pdgfrα lineage ⇨ All lung mesenchyme & part of the lung epithelium

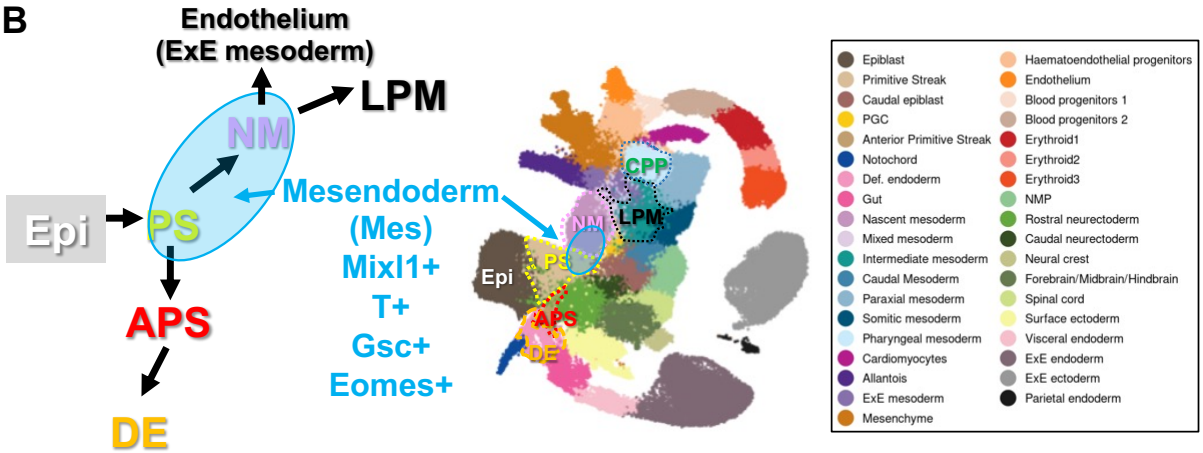

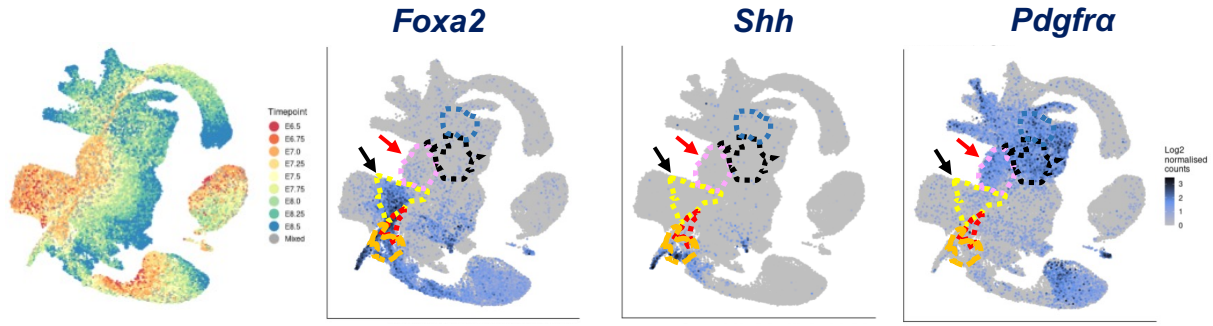

792

793 **Figure S4. Summary of the results and proposed models.** (A) Pluripotent stem cell (PSC)
794 differentiation will be initiated by the Mixl1$^+$ induction and the subsequent temporal expression of
795 an early mesendoderm (ME) marker, Pdgfrα. After that, the late mesendoderm marker marked by
796 Foxa2 will turn on. Pdgfrα and Foxa2-lineage partially overlap at the primitive streak stage during
797 gastrulation. Pdgfrα$^+$ early ME lineage gives rise to the partial lung epithelial cells, most likely by
798 the overlapping Foxa2$^+$ lineage and entire lung mesenchyme through lateral plate mesoderm
799 (LPM) induction and cardiopulmonary lineage (CPP). On the other hand, the Foxa2-lineage gives
800 rise to the whole lung epithelium and about 20% of CPP in early lung development at E12.5~E14.5.
801 Strikingly, the whole lungs, including lung epithelium, mesenchyme, and endothelial cells, were
802 produced solely by donor iPSCs via complementing the Foxa2-lineage's mitotic defective lung
803 niches. It proves that a Foxa2-lineage works as a bona fide lung generative lineage (BFL), enough
804 to generate entire lungs by donor iPSCs via CBC. (B) Top left panel: Schematic diagram of
805 mesendoderm lineage trajectory for lung formation based on the single cell RNA-seq (scRNA-
806 seq) deposited database(Pijuan-Sala et al., 2019). During gastrulation, a bipotent mesendoderm
807 (Mes: rounded blue area) appears in the transition from PS and NM, labeled by *Mixl1, T, Gsc, and*
808 *Eomes*. NM forms lateral plate mesoderm (LPM). Mesendoderm also gives rise to anteriolar PS
809 (APS) and, subsequently, definitive endoderm (DE). Top right panel: Clustering of scRNA-seq
810 provided in the deposited database(Pijuan-Sala et al., 2019). Bottom left panel: Timepoint of
811 scRNA-seq provided in the deposited database(Pijuan-Sala et al., 2019). bottom: *Foxa2* is
812 expressed in the PS (black arrow) and the part of NM (red arrow). In contrast, *Shh* appeared in DE
813 but not in PS, NM, or APS. A few cells showed *Pdgfrα* in PS (black arrow) but most expressed
814 *Pdgfrα* in NM (red arrow) and LPM.
815